

Weak proton capture on ^3He

L.E. Marcucci

Department of Physics, Old Dominion University, Norfolk, Virginia 23529

R. Schiavilla

Jefferson Lab, Newport News, Virginia 23606

and

Department of Physics, Old Dominion University, Norfolk, Virginia 23529

M. Viviani

INFN, Sezione di Pisa, I-56100 Pisa, Italy

A. Kievsky

INFN, Sezione di Pisa, I-56100 Pisa, Italy

S. Rosati

Department of Physics, University of Pisa, I-56100 Pisa, Italy

and

INFN, Sezione di Pisa, I-56100 Pisa, Italy

J.F. Beacom

Physics Department 161-33, California Institute of Technology, Pasadena, California 91125

(October 30, 2018)

Abstract

The astrophysical S -factor for the proton weak capture on ^3He is calculated with correlated-hyperspherical-harmonics bound and continuum wave functions corresponding to realistic Hamiltonians consisting of the Argonne v_{14} or Argonne v_{18} two-nucleon and Urbana-VIII or Urbana-IX three-nucleon interactions. The nuclear weak charge and current operators have vector and axial-vector components, that include one- and many-body terms. All possible multipole transitions connecting any of the $p^3\text{He}$ S- and P-wave channels to the ^4He bound state are considered. The S -factor at a $p^3\text{He}$ center-of-mass energy of 10 keV, close to the Gamow-peak energy, is predicted to be 10.1×10^{-20} keV b with the AV18/UIX Hamiltonian, a factor of $\simeq 4.5$ larger

than the value adopted in the standard solar model. The P-wave transitions are found to be important, contributing about 40 % of the calculated S -factor. The energy dependence is rather weak: the AV18/UIX zero-energy S -factor is 9.64×10^{-20} keV b, only 5 % smaller than the 10 keV result quoted above. The model dependence is also found to be weak: the zero-energy S -factor is calculated to be 10.2×10^{-20} keV b with the older AV14/UVIII model, only 6 % larger than the AV18/UIX result. Our best estimate for the S -factor at 10 keV is therefore $(10.1 \pm 0.6) \times 10^{-20}$ keV b, when the theoretical uncertainty due to the model dependence is included. This value for the calculated S -factor is not as large as determined in fits to the Super-Kamiokande data in which the hep flux normalization is free. However, the precise calculation of the S -factor and the consequent absolute prediction for the hep neutrino flux will allow much greater discrimination among proposed solar neutrino oscillation solutions.

21.45.+v, 27.10.+h, 95.30.Cq

I. INTRODUCTION AND CONCLUSIONS

A. Motivation

Recently, there has been a revival of interest in the reaction ${}^3\text{He}(p, e^+ \nu_e){}^4\text{He}$ [1–6]. This interest has been spurred by the Super-Kamiokande collaboration measurements of the energy spectrum of electrons recoiling from scattering with solar neutrinos [7–9]. Over most of the spectrum, a suppression $\simeq 0.5$ is observed relative to the Standard Solar Model (SSM) predictions [10]. Above 12.5 MeV, however, there is an apparent excess of events. The *hep* process, as the proton weak capture on ${}^3\text{He}$ is known, is the only source of solar neutrinos with energies larger than about 14 MeV—their end-point energy is about 19 MeV. This fact has naturally led to questions about the reliability of calculations of the *hep* weak capture cross section, upon which is based the currently accepted SSM value for the astrophysical *S*-factor at zero energy, 2.3×10^{-20} keV b [11]. In particular, Bahcall and Krastev have shown [1] that a large enhancement, by a factor in the range 25–30, of the SSM *S*-factor value given above would essentially fit the observed excess [7] of recoiling electrons, in any of three different neutrino scenarios—uniform suppression of the ${}^8\text{B}$ flux, vacuum oscillations, and matter-enhanced oscillations [12].

The theoretical description of the *hep* process, as well as that of the neutron and proton radiative captures on ${}^2\text{H}$, ${}^3\text{H}$, and ${}^3\text{He}$, constitute a challenging problem from the standpoint of nuclear few-body theory. Its difficulty can be appreciated by comparing the measured values for the cross section of thermal neutron radiative capture on ${}^1\text{H}$, ${}^2\text{H}$, and ${}^3\text{He}$. Their respective values are: 334.2 ± 0.5 mb [13], 0.508 ± 0.015 mb [14], and 0.055 ± 0.003 mb [15,16]. Thus, in going from $A=2$ to 4 the cross section has dropped by almost four orders of magnitude. These processes are induced by magnetic-dipole transitions between the initial two-cluster state in relative S-wave and the final bound state. In fact, the inhibition of the $A=3$ and 4 captures has been understood for a long time [17]. The ${}^3\text{H}$ and ${}^4\text{He}$ wave functions, denoted, respectively, with Ψ_3 and Ψ_4 are, to a good approximation, eigenfunctions of the magnetic dipole operator $\boldsymbol{\mu}$, namely $\mu_z \Psi_3 \simeq \mu_p \Psi_3$ and $\mu_z \Psi_4 \simeq 0$, where $\mu_p=2.793$ n.m. is the proton magnetic moment (note that the experimental value of the ${}^3\text{H}$ magnetic moment is 2.979 n.m., while ${}^4\text{He}$ has no magnetic moment). These relations would be exact, if the ${}^3\text{H}$ and ${}^4\text{He}$ wave functions were to consist of a symmetric S-wave term only, for example, $\Psi_4 = \phi_4(\text{S}) \det[p \uparrow_1, p \downarrow_2, n \uparrow_3, n \downarrow_4]$. Of course, tensor components in the nuclear interactions generate significant D-state admixtures, that partially spoil this eigenstate property. To the extent that it is approximately satisfied, though, the matrix elements $\langle \Psi_3 | \mu_z | \Psi_{1+2} \rangle$ and $\langle \Psi_4 | \mu_z | \Psi_{1+3} \rangle$ vanish due to orthogonality between the initial and final states. This orthogonality argument fails in the case of the deuteron, since then

$$\mu_z \Psi_2 \simeq (\mu_p - \mu_n) \phi_2(\text{S}) \chi_0^0 \eta_0^1, \quad (1.1)$$

where $\chi_{M_S}^S$ and $\eta_{M_T}^T$ are two-nucleon spin and isospin states, respectively. The magnetic dipole operator can therefore connect the large S-wave component $\phi_2(\text{S})$ of the deuteron to a $T=1$ ${}^1\text{S}_0$ np state (note that the orthogonality between the latter and the deuteron follows from the orthogonality between their respective spin-isospin states).

This quasi-orthogonality, while again invalid in the case of the proton weak capture on protons, is also responsible for inhibiting the *hep* process. Both these reactions are induced

by the Gamow-Teller operator, which differs from the (leading) isovector spin part of the magnetic dipole operator essentially by an isospin rotation. As a result, the *hep* weak capture and *nd*, *pd*, $n^3\text{He}$, and $p^3\text{H}$ radiative captures are extremely sensitive to: (i) small components in the wave functions, particularly the D-state admixtures generated by tensor interactions, and (ii) many-body terms in the electro-weak current operator. For example, two-body current contributions provide, respectively, 50 % and over 90 % of the calculated *pd* [18] and $n^3\text{He}$ [11,19] cross sections at very low energies.

In this respect, the *hep* weak capture is a particularly delicate reaction, for two additional reasons: firstly and most importantly, the one- and two-body current contributions are comparable in magnitude, but of opposite sign [11,20]; secondly, two-body axial currents, specifically those arising from excitation of Δ isobars which have been shown to give the dominant contribution, are model dependent [20–22].

This destructive interference between one- and two-body currents also occurs in the $n^3\text{He}$ (“*hen*”) radiative capture [11,19], with the difference that there the leading components of the two-body currents are model independent, and give a much larger contribution than that associated with the one-body current.

The cancellation in the *hep* process between the one- and two-body matrix elements has the effect of enhancing the importance of P-wave capture channels, which would ordinarily be suppressed. Indeed, one of the results of the present work is that these channels give about 40 % of the *S*-factor calculated value. That the *hep* process could proceed as easily through P- as S-wave capture was not realized—or, at least, not sufficiently appreciated [23]—in all earlier studies of this reaction we are aware of, with the exception of Ref. [4], where it was suggested, on the basis of a very simple one-body reaction model, that the $^3\text{P}_0$ channel may be important.

B. Previous Studies of the *hep* Capture

The history of *hep* cross section calculations has been most recently reviewed by Bahcall and Krastev [1]. The first estimate of the cross section [24] was based on the calculation of the overlap of an s-wave proton continuum wave function and a 1s neutron wave function in ^4He . It produced a large value for the *S*-factor, 630×10^{-20} keV b, and led to the suggestion by Kuzmin [25] that between 20 % and 50 % of the neutrinos in the high-energy end of the flux spectrum could originate from the *hep* reaction. Of course, as already discussed above and originally pointed out by Werntz and Brennan [26], if the ^4He and $p^3\text{He}$ states are approximated, respectively, by $(1s)^4$ and $(1s)^3 2s_c$ configurations ($2s_c$ is the continuum wave function), and antisymmetrized in space, spin, and isospin, then the capture rate vanishes identically. Werntz and Brennan [26] attempted to relate the matrix element of the axial current occurring in the *hep* capture to that of the electromagnetic current occurring in the thermal neutron radiative capture on ^3He , and provided an upper limit for the *hep* *S*-factor, 3.7×10^{-20} keV b, based on an experimental upper limit of 100 μb for the $^3\text{He}(n,\gamma)^4\text{He}$ cross section known at the time.

Werntz and Brennan assumed: (i) the validity of isospin symmetry, apart from differences in the neutron (in *hen* capture) and proton (in *hep* capture) continuum wave functions, which they related to each other via $|\psi_p(r)/\psi_n(r)| \simeq C_0$ (C_0 is the usual Gamow penetration factor); (ii) that two-body currents dominated both the weak and radiative captures, and

that their matrix elements could be put in relation to each other through an isospin rotation. These authors refined their earlier estimate for the *hep* S -factor in a later publication [23], by using hard-sphere phase shifts to obtain a more realistic value for the ratio of the neutron to proton continuum wave functions, and by including the contributions due to P-wave capture channels. These refinements led to an S -factor value, 8.1×10^{-20} keV b, considerably larger than they had obtained previously. They found, though, that the P-waves only contribute at the 10 % level.

Subsequent studies of the *hep* process also attempted to relate it to the *hen* radiative capture, but recognized the importance of D-state components in the ${}^3\text{He}$ and ${}^4\text{He}$ wave functions—these had been ignored in Refs. [23,26]—, and used the Chemtob-Rho prescription [21] (with some short-range modification) for the two-body terms in the electroweak current operator. Tegnér and Bargholtz [27] and Wervelman *et al.* [16] found, using a shell-model description of the initial and final states, that two-body current contributions do not dominate the capture processes, in sharp contrast with the assumptions of Refs. [23,26] and the later conclusions of Refs. [11,19,20]. These two groups as well as Wolfs *et al.* [15] arrived, nevertheless, to contradictory results, due to the different values calculated for the ratio of weak to electromagnetic matrix elements. Tegnér and Bargholtz [27] obtained an S -factor value of $(17 \pm 8) \times 10^{-20}$ keV b, the spread being due to the uncertain experimental value of the thermal neutron capture cross section before 1983. This prediction was sharpened by Wolfs *et al.* [15], who measured the *hen* cross section precisely. They quoted an *hep* S -factor value of $(15.3 \pm 4.7) \times 10^{-20}$ keV b. Wervelman *et al.* [16] also measured the *hen* cross section, reporting a value of $(55 \pm 3) \mu\text{b}$ in excellent agreement with the Wolfs *et al.* measurement of $(54 \pm 6) \mu\text{b}$, but estimated an *hep* S -factor in the range $(57 \pm 8) \times 10^{-20}$ keV b. These discrepancies are presumably due to the schematic wave functions used in the calculations.

In an attempt to reduce the uncertainties in the predicted values for both the radiative and weak capture rates, fully microscopic calculations of these reactions were performed in the early nineties [19,20], based on ground- and scattering-state wave functions obtained variationally from a realistic Hamiltonian with two- and three-nucleon interactions. The main part of the electromagnetic current operator (denoted as “model independent”) was constructed consistently from the two-nucleon interaction model. The less well known (“model dependent”) electroweak currents associated with the excitation of intermediate Δ isobars and with transition couplings, such as the electromagnetic or axial $\rho\pi$ current, were also included. However, it was emphasized that their contribution was to be viewed as numerically uncertain, as very little empirical information is available on their coupling constants and short-range behavior. These studies showed that both the *hen* and *hep* reactions have large (in the case of the radiative capture, dominant) contributions from two-body currents. Indeed, the values obtained with one-body only and full currents for the *hep* S -factor (radiative capture cross section) were, respectively, 5.8×10^{-20} and 1.3×10^{-20} keV b (6 and 112 μb). These results indicated that the common practice of inferring the *hep* S -factor from the measured radiative capture cross section is bound to be misleading, because of different initial-state interactions in the n ${}^3\text{He}$ and p ${}^3\text{He}$ channels, and because of the large contributions associated with the two-body components of the electroweak current operator, and their destructive interference with the one-body current contributions. Yet, the substantial overprediction of the *hen* cross section, 112 μb versus an experimental value of 55 μb , was

unsatisfactory. It became clear that the contributions of the “model dependent” currents, particularly those due to the Δ isobar, were unreasonably large (about $40 \mu\text{b}$ out of the total $112 \mu\text{b}$). It was therefore deemed necessary to include the Δ degrees of freedom explicitly in the nuclear wave functions, rather than eliminate them in favor of effective two-body operators acting on nucleon coordinates, as it had been done in earlier studies. This led to the development of the transition-correlation operator (TCO) method [11]—a scaled-down approach to a full $N+\Delta$ coupled-channel treatment. The radiative capture cross section was now calculated to be between 75 and $80 \mu\text{b}$ [11] (excluding the small contribution of the “uncertain” $\omega\pi\gamma$ current), the spread depending on whether the $\pi N\Delta$ coupling constant in the transition interactions is taken either from experiment or from the quark model. In this approach, the *hep* S -factor was calculated to be in the range between 1.4×10^{-20} and 3.1×10^{-20} keV b [11], the spread due to whether the axial $N\Delta$ coupling was determined by fitting the Gamow-Teller matrix element in tritium β -decay or, again, taken from the quark model (uncertainties in the values of the $\pi N\Delta$ coupling had a much smaller impact). In fact, the SSM value for the *hep* S -factor now quoted in the literature [1,2] is the average of these last two results.

C. Overview of Present Calculations

Improvements in the modeling of two- and three-nucleon interactions and the nuclear weak current, and the significant progress made in the last few years in the description of the bound and continuum four-nucleon wave functions, have prompted us to re-examine the *hep* reaction. The nuclear Hamiltonian has been taken to consist of the Argonne v_{18} two-nucleon [28] and Urbana-IX three-nucleon [29] interactions. To make contact with the earlier studies [11,20], however, and to have some estimate of the model dependence of the results, the older Argonne v_{14} two-nucleon [30] and Urbana-VIII three-nucleon [31] interaction models have also been used. Both these Hamiltonians, the AV18/UIX and AV14/UVIII, reproduce the experimental binding energies and charge radii of the trinucleons and ${}^4\text{He}$ in exact Green’s function Monte Carlo (GFMC) calculations [32,33].

The correlated-hyperspherical-harmonics (CHH) method is used here to solve variationally the bound- and scattering-state four-nucleon problem [34,35]. The binding energy of ${}^4\text{He}$ calculated with the CHH method [34,36] is within 1–2 %, depending on the Hamiltonian model, of that obtained with the GFMC method. The accuracy of the CHH method to calculate scattering states has been successfully verified in the case of the trinucleon systems, by comparing results for a variety of Nd scattering observables obtained by a number of groups using different techniques [37]. Indeed, the numerical uncertainties in the calculation of the trinucleon continuum have been so drastically reduced that Nd scattering observables can now be used to directly study the sensitivity to two- and three-nucleon interaction models—the A_y “puzzle” constitutes an excellent example of this type of studies [38].

Studies along similar lines show [39] that the CHH solutions for the four-nucleon continuum are also highly accurate. The CHH predictions [35] for the n ${}^3\text{H}$ total elastic cross section, $\sigma_T = \pi (|a_s|^2 + 3|a_t|^2)$, and coherent scattering length, $a_c = a_s/4 + 3a_t/4$, measured by neutron interferometry techniques— a_s and a_t are the singlet and triplet scattering lengths—have been found to be in excellent agreement with the corresponding experimental values. The n ${}^3\text{H}$ cross section is known over a rather wide energy range, and its extrapola-

tion to zero energy is not problematic [40]. The situation is different for the $p^3\text{He}$ channel, for which the scattering lengths have been determined from effective range extrapolations of data taken above 1 MeV, and are therefore somewhat uncertain, $a_s = (10.8 \pm 2.6)$ fm [41] and $a_t = (8.1 \pm 0.5)$ fm [41] or (10.2 ± 1.5) fm [27]. Nevertheless, the CHH results are close to the experimental values above. For example, the AV18/UIX Hamiltonian predicts [35] $a_s = 10.1$ fm and $a_t = 9.13$ fm.

In Refs. [11,20] variational Monte Carlo (VMC) wave functions had been used to describe both bound and scattering states. The triplet scattering length was found to be 10.1 fm with the AV14/UVIII Hamiltonian model, in satisfactory agreement with the experimental determination and the value obtained with the more accurate CHH wave functions. However, the present work includes all S- and P-wave channels, namely $^1\text{S}_0$, $^3\text{S}_1$, $^3\text{P}_0$, $^1\text{P}_1$, $^3\text{P}_1$, and $^3\text{P}_2$, while all previous works only retained the $^3\text{S}_1$ channel, which was thought, erroneously, to be the dominant one.

The nuclear weak current consists of vector and axial-vector parts, with corresponding one-, two-, and many-body components. The weak vector current is constructed from the isovector part of the electromagnetic current, in accordance with the conserved-vector-current (CVC) hypothesis. Two-body weak vector currents have “model-independent” and “model-dependent” components. The model-independent terms are obtained from the nucleon-nucleon interaction, and by construction satisfy current conservation with it. The leading two-body weak vector current is the “ π -like” operator, obtained from the isospin-independent spin-spin and tensor nucleon-nucleon interactions. The latter also generate an isovector “ ρ -like” current, while additional isovector two-body currents arise from the isospin-independent and isospin-dependent central and momentum-dependent interactions. These currents are short-ranged, and numerically far less important than the π -like current. With the exception of the ρ -like current, they have been neglected in the present work. The model-dependent currents are purely transverse, and therefore cannot be directly linked to the underlying two-nucleon interaction. The present calculation includes the isovector currents associated with excitation of Δ isobars which, however, are found to give a rather small contribution in weak-vector transitions, as compared to that due to the π -like current. The π -like and ρ -like weak vector charge operators have also been retained in the present study.

The leading two- and many-body terms in the axial current, in contrast to the case of the weak vector (or electromagnetic) current, are those due to Δ -isobar excitation, which are treated within the TCO scheme. This scheme has in fact been extended [42] to include three-body connected terms which were neglected in the earlier work [11]. The axial charge operator includes the long-range pion-exchange term [43], required by low-energy theorems and the partially-conserved-axial-current relation, as well as the (expected) leading short-range terms constructed from the central and spin-orbit components of the nucleon-nucleon interaction, following a prescription due to Riska and collaborators [44].

The largest model dependence is in the weak axial current. To minimize it, the poorly known $N \rightarrow \Delta$ transition axial coupling constant has been adjusted to reproduce the experimental value of the Gamow-Teller matrix element in tritium β -decay. While this procedure is inherently model dependent, its actual model dependence is in fact very weak, as has been shown in Ref. [45]. The analysis carried out there could be extended to the present case.

D. Conclusions

We present here a discussion of the results for the astrophysical S -factor and their implications for the Super-Kamiokande (SK) solar neutrino spectrum.

1. Results for the S -factor

Our results for the astrophysical S -factor, defined as

$$S(E) = E \sigma(E) \exp(4 \pi \alpha / v_{\text{rel}}) , \quad (1.2)$$

where $\sigma(E)$ is the hep cross section at center-of-mass energy E , v_{rel} is the p ^3He relative velocity, and α is the fine structure constant, are reported in Table I. By inspection of the table, we note that: (i) the energy dependence is rather weak: the value at 10 keV is only about 4 % larger than that at 0 keV; (ii) the P-wave capture states are found to be important, contributing about 40 % of the calculated S -factor. However, the contributions from D-wave channels are expected to be very small. We have verified explicitly that they are indeed small in $^3\text{D}_1$ capture. (iii) The many-body axial currents associated with Δ excitation play a crucial role in the (dominant) $^3\text{S}_1$ capture, where they reduce the S -factor by more than a factor of four; thus the destructive interference between the one- and many-body current contributions, first obtained in Ref. [20], is confirmed in the present study, based on more accurate wave functions. The (suppressed) one-body contribution comes mostly from transitions involving the D-state components of the ^3He and ^4He wave functions, while the many-body contributions are predominantly due to transitions connecting the S-state in ^3He to the D-state in ^4He , or viceversa.

It is important to stress the differences between the present and all previous studies. Apart from ignoring, or at least underestimating, the contribution due to P-waves, the latter only considered the long-wavelength form of the weak multipole operators, namely, their $q=0$ limit, where q is the magnitude of the momentum transfer. In $^3\text{P}_0$ capture, for example, only the C_0 -multipole, associated with the weak axial charge, survives in this limit, and the corresponding S -factor is calculated to be 2.2×10^{-20} keV b, including two-body contributions. However, when the transition induced by the longitudinal component of the axial current (via the L_0 -multipole, which vanishes at $q=0$) is also taken into account, the S -factor becomes 0.82×10^{-20} keV b, because of destructive interference between the C_0 and L_0 matrix elements (see discussion in Sec. II C). Thus use of the long-wavelength approximation in the calculation of the hep cross section leads to inaccurate results.

Finally, besides the differences listed above, the present calculation also improves that of Ref. [11] in a number of other important respects: firstly, it uses CHH wave functions, corresponding to the latest generation of realistic interactions; secondly, the model for the nuclear weak current has been extended to include the axial charge as well as the vector charge and current operators. Thirdly, the one-body operators now take into account the $1/m^2$ relativistic corrections, which had previously been neglected. In $^3\text{S}_1$ capture, for example, these terms increase by 25 % the dominant (but suppressed) L_1 and E_1 matrix elements calculated with the (lowest order) Gamow-Teller operator. These improvements in the treatment of the one-body axial current indirectly affect also the contributions of

the Δ -excitation currents, since the $N\Delta$ transition axial coupling constant is determined by reproducing the Gamow-Teller matrix element in tritium β -decay, as discussed in Sec. IV E below.

The chief conclusion of the present work is that the *hep* S -factor is predicted to be $\simeq 4.5$ times larger than the value adopted in the SSM. This enhancement, while very significant, is smaller than that first suggested in Refs. [1,3], and then reconsidered by the SK collaboration in Ref. [9]. A discussion of the implications of our results for the SK solar neutrino spectrum is given below.

Even though our result is inherently model dependent, it is unlikely that the model dependence is large enough to accommodate a drastic increase in the value obtained here. Indeed, calculations using Hamiltonians based on the AV18 two-nucleon interaction only and the older AV14/UVIII two- and three-nucleon interactions predict zero energy S -factor values of 12.1×10^{-20} keV b and 10.2×10^{-20} keV b, respectively. It should be stressed, however, that the AV18 model, in contrast to the AV14/UVIII, does not reproduce the experimental binding energies and low-energy scattering parameters of the three- and four-nucleon systems. The AV14/UVIII prediction is only 6 % larger than the AV18/UIX zero-energy result. This 6 % variation should provide a fairly realistic estimate of the theoretical uncertainty due to the model dependence. It would be very valuable, though, to repeat the present study with a Hamiltonian consisting of the CD-Bonn interaction [46] which, in contrast to the AV14 and AV18 models, has strongly non-local central and tensor components. We would expect the CD-Bonn calculation to predict an S -factor value close to that reported here, provided the axial current in that calculation were again constrained to reproduce the known Gamow-Teller matrix element in tritium β -decay [45].

To conclude, our best estimate for the S -factor at 10 keV c.m. energy is therefore $(10.1 \pm 0.6) \times 10^{-20}$ keV b.

2. Effect on the Super-Kamiokande Solar Neutrino Spectrum

Super-Kamiokande (SK) detects solar neutrinos by neutrino-electron scattering. The energy is shared between the outgoing neutrino and scattered electron, leading to a very weak correlation between the incoming neutrino energy and the measured electron energy. The electron angle relative to the solar direction is also measured, which would in principle allow reconstruction of the incoming neutrino energy. However, the kinematic range of the angle is very forward, and is comparable to the angular resolution of the detector. Furthermore, event-by-event reconstruction of the neutrino energy would be prevented by the detector background. Above its threshold of several MeV, SK is sensitive to the ${}^8\text{B}$ electron neutrinos. These have a total flux of $5.15 \times 10^6 \text{ cm}^{-2} \text{ s}^{-1}$ in the SSM [10]. While the flux is uncertain to about 15 %, primarily due to the nuclear-physics uncertainties in the ${}^7\text{Be}(p,\gamma){}^8\text{B}$ cross section, the spectral shape is more precisely known [47].

The SK results are presented as the ratio of the measured electron spectrum to that expected in the SSM with no neutrino oscillations. Over most of the spectrum, this ratio is constant at $\simeq 0.5$. At the highest energies, however, an excess relative to $0.5 \times \text{SSM}$ is seen (though it has diminished in successive data sets). The SK 825-day data, determined graphically from Fig. 8 of Ref. [9], are shown by the points in Fig. 1 (the error bars denote the combined statistical and systematic error). The excess above 12.5 MeV may be interpreted

as neutrino-energy dependence in the neutrino oscillation probability that is not completely washed out in the electron spectrum. This excess has also been interpreted as possible evidence for a large *hep* flux [1,3,9] (though note that the data never exceeds the *full* SSM expectation from ${}^8\text{B}$ neutrinos). In the SSM, the total *hep* flux is very small, $2.10 \times 10^3 \text{ cm}^{-2} \text{ s}^{-1}$. However, its endpoint energy is higher than for the ${}^8\text{B}$ neutrinos, 19 MeV instead of about 14 MeV, so that the *hep* neutrinos may be seen at the highest energies. This is somewhat complicated by the energy resolution of SK, which allows ${}^8\text{B}$ events beyond their nominal endpoint. The ratio of the *hep* flux to its value in the SSM (based on the *hep* S-factor prediction of Ref. [11]) will be denoted by α , defined as

$$\alpha \equiv \frac{S_{\text{new}}}{S_{\text{SSM}}} \times P_{\text{osc}} , \quad (1.3)$$

where P_{osc} is the *hep*-neutrino suppression constant. In the present work, $\alpha = (10.1 \times 10^{-20} \text{ keV b}) / (2.3 \times 10^{-20} \text{ keV b}) = 4.4$, if *hep* neutrino oscillations are ignored. The solid lines in Fig. 1 indicate the effect of various values of α on the ratio of the electron spectrum with both ${}^8\text{B}$ and *hep* to that with only ${}^8\text{B}$ (the SSM). Though some differences are expected in the *hep* spectral shape due to P-wave contributions, here we simply use the standard *hep* spectrum shape [48]. In calculating this ratio, the ${}^8\text{B}$ flux in the numerator has been suppressed by 0.47, the best-fit constant value for the observed suppression. If the *hep* neutrinos are suppressed by $\simeq 0.5$, then $\alpha = 2.2$. Two other arbitrary values of α (10 and 20) are shown for comparison. As for the SK data, the results are shown as a function of the total electron energy in 0.5 MeV bins. The last bin, shown covering 14 – 15 MeV, actually extends to 20 MeV. The SK energy resolution was approximated by convolution with a Gaussian of energy-dependent width, chosen to match the SK LINAC calibration data [49].

The effects of a larger *hep* flux should be compared to other possible distortions of the ratio. The data show no excess at low energies, thus limiting the size of a neutrino magnetic moment contribution to the scattering [50]. The ${}^8\text{B}$ neutrino energy spectrum has recently been remeasured by Ortiz *et al.* [51] and their spectrum is significantly larger at high energies than that of Ref. [47]. Relative to the standard spectrum, this would cause an increase in the ratio at high energies comparable to the $\alpha = 4.4$ case. The measured electron spectrum is very steep, and the fraction of events above 12.5 MeV is only $\sim 1\%$ of the total above threshold. Thus, an error in either the energy scale or resolution could cause an apparent excess of events at high energy. However, these are known precisely from the SK LINAC [49] calibration; an error in either could explain the data only if it were at about the 3- or 4-sigma level [9].

The various neutrino oscillation solutions can be distinguished by their neutrino-energy dependence, though the effects on the electron spectrum are small. Generally, the ratio is expected to be rising at high energies, much like the effect of an increased *hep* flux. The present work predicts $\alpha = 4.4$ (and $\alpha = 2.2$ if the *hep* neutrinos oscillate). From Fig. 1, this effect is smaller than the distortion seen in the data or found in Refs. [1,3,9], where the *hep* flux was fitted as a free parameter. However, the much more important point is that this is an *absolute* prediction. Fixing the value of α will significantly improve the ability of SK to identify the correct oscillation solution.

In the remainder of the paper we provide details of the calculation leading to these conclusions. In Sec. II we derive the *hep* cross section in terms of reduced matrix elements of

the weak current multipole operators. In Sec. III we discuss the calculation of the bound- and scattering-state wave functions with the CHH method, and summarize a number of results obtained for the ${}^4\text{He}$ binding energy and p ${}^3\text{He}$ elastic scattering observables, comparing them to experimental data. In Sec. IV we review the model for the nuclear weak current and charge operators, while in Sec. V we provide details about the calculation of the matrix elements and resulting cross section. Finally, in Sec. VI we summarize and discuss our results.

II. CROSS SECTION

In this section we sketch the derivation of the cross section for the p ${}^3\text{He}$ weak capture process. The center-of-mass (c.m.) energies of interest are of the order of 10 keV—the Gamow-peak energy is 10.7 keV—and it is therefore convenient to expand the p ${}^3\text{He}$ scattering state into partial waves, and perform a multipole decomposition of the nuclear weak charge and current operators. The present study includes S- and P-wave capture channels, i.e. the ${}^1\text{S}_0$, ${}^3\text{S}_1$, ${}^3\text{P}_0$, ${}^1\text{P}_1$, ${}^3\text{P}_1$, and ${}^3\text{P}_2$ states in the notation ${}^{2S+1}\text{L}_J$ with $S = 0, 1$, and retains all contributing multipoles connecting these states to the $J^\pi=0^+$ ${}^4\text{He}$ ground state. The relevant formulas are given in the next three subsections. Note that the ${}^1\text{P}_1$ and ${}^3\text{P}_1$, and ${}^3\text{S}_1$ and ${}^3\text{D}_1$ channels are coupled. For example, a pure ${}^1\text{P}_1$ incoming wave will produce both ${}^1\text{P}_1$ and ${}^3\text{P}_1$ outgoing waves. The degree of mixing is significant, particularly for the P-waves, as discussed in Sec. III C.

A. The Transition Amplitude

The capture process ${}^3\text{He}(p, e^+ \nu_e){}^4\text{He}$ is induced by the weak interaction Hamiltonian [52]

$$H_W = \frac{G_V}{\sqrt{2}} \int d\mathbf{x} e^{-i(\mathbf{p}_e + \mathbf{p}_\nu) \cdot \mathbf{x}} l_\sigma j^\sigma(\mathbf{x}), \quad (2.1)$$

where G_V is the Fermi coupling constant ($G_V = 1.14939 \cdot 10^{-5} \text{ GeV}^{-2}$ [53]), l_σ is the leptonic weak current

$$l_\sigma = \bar{u}_\nu \gamma_\sigma (1 - \gamma_5) v_e \equiv (\bar{l}_0, -\mathbf{l}), \quad (2.2)$$

and $j^\sigma(\mathbf{x})$ is the hadronic weak current density. The positron and (electron) neutrino momenta and spinors are denoted, respectively, by \mathbf{p}_e and \mathbf{p}_ν , and v_e and u_ν . The Bjorken and Drell [54] conventions are used for the metric tensor $g^{\sigma\tau}$ and γ -matrices. However, the spinors are normalized as $v_e^\dagger v_e = u_\nu^\dagger u_\nu = 1$.

The transition amplitude in the c.m. frame is then given by

$$\langle f | H_W | i \rangle = \frac{G_V}{\sqrt{2}} l^\sigma \langle -\mathbf{q}; {}^4\text{He} | j_\sigma^\dagger(\mathbf{q}) | \mathbf{p}; p {}^3\text{He} \rangle, \quad (2.3)$$

where $\mathbf{q} = \mathbf{p}_e + \mathbf{p}_\nu$, $|\mathbf{p}; p {}^3\text{He}\rangle$ and $|\mathbf{q}; {}^4\text{He}\rangle$ represent the p ${}^3\text{He}$ scattering state with relative momentum \mathbf{p} and ${}^4\text{He}$ bound state recoiling with momentum $-\mathbf{q}$, respectively, and

$$j^\sigma(\mathbf{q}) = \int d\mathbf{x} e^{i\mathbf{q}\cdot\mathbf{x}} j^\sigma(\mathbf{x}) \equiv (\rho(\mathbf{q}), \mathbf{j}(\mathbf{q})) . \quad (2.4)$$

The dependence of the amplitude upon the spin-projections of the proton and ${}^3\text{He}$ is understood. It is useful to perform a partial-wave expansion of the p ${}^3\text{He}$ scattering wave function

$$\Psi_{\mathbf{p}, s_1 s_3}^{(+)} = \sqrt{4\pi} \sum_{LSJJ_z} \sqrt{2L+1} i^L \langle \frac{1}{2} s_1, \frac{1}{2} s_3 | SJ_z \rangle \langle SJ_z, L0 | JJ_z \rangle \bar{\Psi}_{1+3}^{LSJJ_z} , \quad (2.5)$$

with

$$\bar{\Psi}_{1+3}^{LSJJ_z} = e^{i\sigma_L} \sum_{L'S'} [1 - i R^J]_{LS, L'S'}^{-1} \Psi_{1+3}^{L'S'JJ_z} , \quad (2.6)$$

where s_1 and s_3 are the proton and ${}^3\text{He}$ spin projections, L , S , and J are the relative orbital angular momentum, channel spin ($S=0,1$), and total angular momentum ($\mathbf{J} = \mathbf{L} + \mathbf{S}$), respectively, R^J is the R -matrix in channel J , and σ_L is the Coulomb phase shift,

$$\sigma_L = \arg[\Gamma(L+1+i\eta)] , \quad (2.7)$$

$$\eta = \frac{2\alpha}{v_{\text{rel}}} . \quad (2.8)$$

Here α is the fine-structure constant and v_{rel} is the p ${}^3\text{He}$ relative velocity, $v_{\text{rel}} = p/\mu$, μ being the reduced mass, $\mu = mm_3/(m+m_3)$ (m and m_3 are the proton and ${}^3\text{He}$ rest masses, respectively). Note that $\Psi^{(+)}$ has been constructed to satisfy outgoing wave boundary conditions, and that the spin quantization axis has been chosen to lie along $\hat{\mathbf{p}}$, which defines the z -axis. Finally, the scattering wave function $\Psi_{1+3}^{LSJJ_z}$ as well as the ${}^4\text{He}$ wave function Ψ_4 are obtained variationally with the correlated-hyperspherical-harmonics (CHH) method, as described in Sec. III.

The transition amplitude is then written as

$$\begin{aligned} \langle f | H_W | i \rangle &= \frac{G_V}{\sqrt{2}} \sqrt{4\pi} \sum_{LSJJ_z} \sqrt{2L+1} i^L \langle \frac{1}{2} s_1, \frac{1}{2} s_3 | SJ_z \rangle \langle SJ_z, L0 | JJ_z \rangle \\ &\times \left[\bar{l}_0 \langle \Psi_4 | \rho^\dagger(\mathbf{q}) | \bar{\Psi}_{1+3}^{LSJJ_z} \rangle - \sum_{\lambda=0, \pm 1} l_\lambda \langle \Psi_4 | \hat{\mathbf{e}}_{q\lambda}^* \cdot \mathbf{j}^\dagger(\mathbf{q}) | \bar{\Psi}_{1+3}^{LSJJ_z} \rangle \right] , \end{aligned} \quad (2.9)$$

where, with the future aim of a multipole decomposition of the weak transition operators, the lepton vector \mathbf{l} has been expanded as

$$\mathbf{l} = \sum_{\lambda=0, \pm 1} l_\lambda \hat{\mathbf{e}}_{q\lambda}^* , \quad (2.10)$$

with $l_\lambda = \hat{\mathbf{e}}_{q\lambda} \cdot \mathbf{l}$, and

$$\hat{\mathbf{e}}_{q0} \equiv \hat{\mathbf{e}}_{q3} , \quad (2.11)$$

$$\hat{\mathbf{e}}_{q\pm 1} \equiv \mp \frac{1}{\sqrt{2}} (\hat{\mathbf{e}}_{q1} \pm i \hat{\mathbf{e}}_{q2}) . \quad (2.12)$$

The orthonormal basis $\hat{\mathbf{e}}_{q1}, \hat{\mathbf{e}}_{q2}, \hat{\mathbf{e}}_{q3}$ is defined by $\hat{\mathbf{e}}_{q3} = \hat{\mathbf{q}}$, $\hat{\mathbf{e}}_{q2} = \mathbf{p} \times \mathbf{q} / |\mathbf{p} \times \mathbf{q}|$, $\hat{\mathbf{e}}_{q1} = \hat{\mathbf{e}}_{q2} \times \hat{\mathbf{e}}_{q3}$.

B. The Multipole Expansion

Standard techniques [52] can now be used to perform the multipole expansion of the weak charge and current matrix elements occurring in Eq. (2.9). The spin quantization axis is along $\hat{\mathbf{p}}$ rather than along $\hat{\mathbf{q}}$. Thus, we first express the states quantized along $\hat{\mathbf{p}}$ as linear combinations of those quantized along $\hat{\mathbf{q}}$:

$$|J J_z\rangle_{\hat{\mathbf{p}}} = \sum_{J'_z} D_{J'_z J_z}^J(-\phi, \theta, \phi) |J J'_z\rangle_{\hat{\mathbf{q}}}, \quad (2.13)$$

where $D_{J'_z J_z}^J$ are standard rotation matrices [52,55] and the angles θ and ϕ specify the direction $\hat{\mathbf{q}}$. We then make use of the transformation properties under rotations of irreducible tensor operators to arrive at the following expressions:

$$\langle \Psi_4 | \rho^\dagger(\mathbf{q}) | \bar{\Psi}_{1+3}^{LSJJ_z} \rangle = \sqrt{4\pi} (-i)^J (-)^{J-J_z} D_{-J_z, 0}^J(-\phi, -\theta, \phi) C_J^{LSJ}(q), \quad (2.14)$$

$$\langle \Psi_4 | \hat{\mathbf{e}}_{q0}^* \cdot \mathbf{j}^\dagger(\mathbf{q}) | \bar{\Psi}_{1+3}^{LSJJ_z} \rangle = \sqrt{4\pi} (-i)^J (-)^{J-J_z} D_{-J_z, 0}^J(-\phi, -\theta, \phi) L_J^{LSJ}(q), \quad (2.15)$$

$$\begin{aligned} \langle \Psi_4 | \hat{\mathbf{e}}_{q\lambda}^* \cdot \mathbf{j}^\dagger(\mathbf{q}) | \bar{\Psi}_{1+3}^{LSJJ_z} \rangle &= -\sqrt{2\pi} (-i)^J (-)^{J-J_z} D_{-J_z, -\lambda}^J(-\phi, -\theta, \phi) \\ &\times [\lambda M_J^{LSJ}(q) + E_J^{LSJ}(q)]. \end{aligned} \quad (2.16)$$

Here $\lambda = \pm 1$, and C_J^{LSJ} , L_J^{LSJ} , E_J^{LSJ} and M_J^{LSJ} denote the reduced matrix elements of the Coulomb (C), longitudinal (L), transverse electric (E) and transverse magnetic (M) multipole operators, explicitly given by [52]

$$C_{u_z}(q) = \int d\mathbf{x} \rho(\mathbf{x}) j_l(qx) Y_{u_z}(\hat{\mathbf{x}}), \quad (2.17)$$

$$L_{u_z}(q) = \frac{i}{q} \int d\mathbf{x} \mathbf{j}(\mathbf{x}) \cdot \nabla j_l(qx) Y_{u_z}(\hat{\mathbf{x}}), \quad (2.18)$$

$$E_{u_z}(q) = \frac{1}{q} \int d\mathbf{x} \mathbf{j}(\mathbf{x}) \cdot \nabla \times j_l(qx) \mathbf{Y}_{u_z}^{l1}, \quad (2.19)$$

$$M_{u_z}(q) = \int d\mathbf{x} \mathbf{j}(\mathbf{x}) \cdot j_l(qx) \mathbf{Y}_{u_z}^{l1}, \quad (2.20)$$

where $\mathbf{Y}_{u_z}^{l1}$ are vector spherical harmonics.

Finally, it is useful to consider the transformation properties under parity of the multipole operators. The weak charge/current operators have components of both scalar/polar-vector (V) and pseudoscalar/axial-vector (A) character, and hence

$$T_{u_z} = T_{u_z}(\text{V}) + T_{u_z}(\text{A}), \quad (2.21)$$

where T_{u_z} is any of the multipole operators above. Obviously, the parity of l th-pole V-operators is opposite of that of l th-pole A-operators. The parity of Coulomb, longitudinal, and electric l th-pole V-operators is $(-)^l$, while that of magnetic l th-pole V-operators is $(-)^{l+1}$.

C. The Cross Section

The cross section for the ${}^3\text{He}(p, e^+\nu_e){}^4\text{He}$ reaction at a c.m. energy E is given by

$$\begin{aligned} \sigma(E) &= \int 2\pi \delta\left(\Delta m + E - \frac{q^2}{2m_4} - E_e - E_\nu\right) \frac{1}{v_{\text{rel}}} \\ &\quad \times \frac{1}{4} \sum_{s_e s_\nu} \sum_{s_1 s_3} |\langle f | H_W | i \rangle|^2 \frac{d\mathbf{p}_e}{(2\pi)^3} \frac{d\mathbf{p}_\nu}{(2\pi)^3}, \end{aligned} \quad (2.22)$$

where $\Delta m = m + m_3 - m_4 = 19.287$ MeV (m_4 is the ${}^4\text{He}$ rest mass), and v_{rel} is the p ${}^3\text{He}$ relative velocity defined above. It is convenient to write:

$$\frac{1}{4} \sum_{s_e s_\nu} \sum_{s_1 s_3} |\langle f | H_W | i \rangle|^2 = (2\pi)^2 G_V^2 L_{\sigma\tau} N^{\sigma\tau}, \quad (2.23)$$

where the lepton tensor $L^{\sigma\tau}$ is defined as

$$\begin{aligned} L^{\sigma\tau} &\equiv \frac{1}{2} \sum_{s_e s_\nu} l^\sigma l^{\tau*} = \frac{1}{2} \text{tr} \left[\gamma^\sigma (1 - \gamma_5) \frac{(\not{p}_e - m_e)}{2E_e} \gamma^\tau (1 - \gamma_5) \frac{\not{p}_\nu}{2E_\nu} \right] \\ &= v_e^\sigma v_\nu^\tau + v_\nu^\sigma v_e^\tau - g^{\sigma\tau} v_e \cdot v_\nu + i \epsilon^{\sigma\alpha\tau\beta} v_{e,\alpha} v_{\nu,\beta}, \end{aligned} \quad (2.24)$$

with $\epsilon^{0123} = -1$, $v_e^\sigma = p_e^\sigma/E_e$ and $v_\nu^\sigma = p_\nu^\sigma/E_\nu$. The nuclear tensor $N^{\sigma\tau}$ is defined as

$$N^{\sigma\tau} \equiv \sum_{s_1 s_3} W^\sigma(\mathbf{q}; s_1 s_3) W^{\tau*}(\mathbf{q}; s_1 s_3), \quad (2.25)$$

where

$$W^{\sigma=0}(\mathbf{q}; s_1 s_3) = \sum_{LSJ} X_0^{LSJ}(\hat{\mathbf{q}}; s_1 s_3) C_J^{LSJ}(q), \quad (2.26)$$

$$W^{\sigma=3}(\mathbf{q}; s_1 s_3) = \sum_{LSJ} X_0^{LSJ}(\hat{\mathbf{q}}; s_1 s_3) L_J^{LSJ}(q), \quad (2.27)$$

$$W^{\sigma=\pm 1}(\mathbf{q}; s_1 s_3) = -\frac{1}{\sqrt{2}} \sum_{LSJ} X_{\mp 1}^{LSJ}(\hat{\mathbf{q}}; s_1 s_3) [\pm M_J^{LSJ}(q) + E_J^{LSJ}(q)]. \quad (2.28)$$

The dependence upon the direction $\hat{\mathbf{q}}$ and proton and ${}^3\text{He}$ spin projections s_1 and s_3 is contained in the functions X_λ^{LSJ} given by

$$\begin{aligned} X_\lambda^{LSJ}(\hat{\mathbf{q}}; s_1 s_3) &= \sum_{J_z} \sqrt{2L+1} i^L (-i)^J (-)^{J-J_z} \langle \frac{1}{2} s_1, \frac{1}{2} s_3 | S J_z \rangle \langle S J_z, L 0 | J J_z \rangle \\ &\quad \times D_{-J_z, \lambda}^J(-\phi, -\theta, \phi), \end{aligned} \quad (2.29)$$

with $\lambda = 0, \pm 1$. Note that the Cartesian components of the lepton and nuclear tensors ($\sigma, \tau = 1, 2, 3$) are relative to the orthonormal basis $\hat{\mathbf{e}}_{q1}, \hat{\mathbf{e}}_{q2}, \hat{\mathbf{e}}_{q3}$, defined at the end of Sec. II A.

The expression for the nuclear tensor can be further simplified by making use of the reduction formulas for the product of rotation matrices [55]. In fact, it can easily be shown that the dependence of $N^{\sigma\tau}$ upon the angle $\cos\theta = \hat{\mathbf{p}} \cdot \hat{\mathbf{q}}$ can be expressed in terms of Legendre polynomials $P_n(\cos\theta)$ and associated Legendre functions $P_n^m(\cos\theta)$ with $m = 1, 2$. However, given the large number of channels included in the present study (all S- and P-wave capture states), the resulting equations for $N^{\sigma\tau}$ are not particularly illuminating, and will not be given here. Indeed, the calculation of the cross section, Eq. (2.22), is carried out numerically with the techniques discussed in Sec. V B.

It is useful, though, to discuss the simple case in which only the contributions involving transitions from the 3S_1 and 3P_0 capture states are considered. In the limit $q = 0$, one then finds

$$\sigma(E) \simeq \frac{2}{\pi} \frac{G_V^2}{v_{\text{rel}}} m_e^5 f_0(E) \left[|L_1^{011}(A)|^2 + |E_1^{011}(A)|^2 + |C_0^{110}(A)|^2 \right], \quad (2.30)$$

where $L_1^{011}(A)$ and $E_1^{011}(A)$ are the longitudinal and transverse electric axial current reduced matrix elements (from 3S_1 capture), and $C_0^{110}(A)$ is the Coulomb axial charge reduced matrix element (from 3P_0 capture) at $q=0$. Here the ‘‘Fermi function’’ $f_0(E)$ is defined as

$$f_0(E) = \int_1^{x_0} dx x \sqrt{x^2 - 1} (x_0 - x)^2, \quad (2.31)$$

with $x_0 = (\Delta m + E)/m_e$. The expression in Eq. (2.30) can easily be related, *mutatis mutandis*, to that given in Ref. [20].

Although the $q=0$ approximation can appear to be adequate for the *hep* reaction, for which $q \leq 20$ MeV/c and $qR \simeq 0.14$ or less (R being the ${}^4\text{He}$ radius), the expression for the cross section given in Eq. (2.30) is in fact inaccurate. To elaborate this point further, consider the 3P_0 capture. The long-wavelength forms of the $C_0(q; A)$ and $L_0(q; A)$ multipoles, associated with the axial charge and longitudinal component of the axial current, are constant and linear in q , respectively, as can be easily inferred from Eqs. (2.17)–(2.18). The corresponding reduced matrix elements are, to leading order in q ,

$$C_0^{110}(q; A) \simeq c_0 + \dots, \quad (2.32)$$

$$L_0^{110}(q; A) \simeq l_0 q + \dots, \quad (2.33)$$

where $c_0 = C_0^{110}(A)$ in the notation of Eq. (2.30). The 3P_0 capture cross section can be written, in this limit, as

$$\sigma(E; {}^3P_0) \simeq \frac{2}{\pi} \frac{G_V^2}{v_{\text{rel}}} m_e^5 \left[f_0(E) |c_0|^2 + f_1(E) m_e^2 |l_0|^2 - 2 f_2(E) m_e \Re(c_0^* l_0) \right]. \quad (2.34)$$

When the full model for the nuclear axial charge and current is considered, the constants c_0 and l_0 , at zero p ³He relative energy, are calculated to be $c_0 = i0.043 \text{ fm}^{3/2}$ and $l_0 = i0.197 \text{ fm}^{5/2}$ (note that they are purely imaginary at $E = 0$). The ‘‘Fermi functions’’ $f_0(E)$, $f_1(E)$, and $f_2(E)$, that arise after integration over the phase space, at $E = 0$ have the values $f_0(0) = 2.54 \times 10^6$, $f_1(0) = 3.61 \times 10^9$, and $f_2(0) = 9.59 \times 10^7$. The zero energy S -factor obtained by including only the term c_0 is 2.2×10^{-20} keV b. However, when both the c_0 and l_0 terms are retained, it becomes 0.68×10^{-20} keV b.

In fact, this last value is still inaccurate: when not only the leading, but also the next-to-leading order terms are considered in the expansion of the multipoles in powers of q (see Sec. VB), the S -factor for ${}^3\text{P}_0$ capture increases to 0.82×10^{-20} keV b, its fully converged value. The conclusion of this discussion is that use of the long-wavelength approximation in the hep reaction leads to erroneous results.

Similar considerations also apply to the case of ${}^3\text{S}_1$ capture: at values of q different from zero, the transition can be induced not only by the axial current via the $E_1(\text{A})$ and $L_1(\text{A})$ multipoles, but also by the axial charge and vector current via the $C_1(\text{A})$ and $M_1(\text{V})$ multipoles. While the contribution of $M_1(\text{V})$ is much smaller than that of the leading $E_1(\text{A})$ and $L_1(\text{A})$, the contribution of $C_1(\text{A})$ is relatively large, and its interference with that of $L_1(\text{A})$ cannot be neglected. This point is further discussed in Sec. VIB.

As a final remark, we note that the general expression for the cross section in Eq. (2.22) as follows from Eqs. (2.23)–(2.29) contains interference terms among the reduced matrix elements of multipole operators connecting different capture channels. However, these interference contributions have been found to account for less than 2 % of the total S -factor at zero p ${}^3\text{He}$ c.m. energy.

III. BOUND- AND SCATTERING-STATE WAVE FUNCTIONS

The ${}^4\text{He}$ bound-state and p ${}^3\text{He}$ scattering-state wave functions are obtained variationally with the correlated-hyperspherical-harmonics (CHH) method from realistic Hamiltonians consisting of the Argonne v_{18} two-nucleon [28] and Urbana-IX three-nucleon [29] interactions (the AV18/UIX model), or the older Argonne v_{14} two-nucleon [30] and Urbana-VIII three-nucleon [31] interactions (the AV14/UVIII model). The CHH method, as implemented in the calculations reported in the present work, has been developed by Viviani, Kievsky, and Rosati in Refs. [34,35,56,57]. Here, it will be reviewed briefly for completeness, and a summary of relevant results obtained for the three- and four-nucleon bound-state properties, and p ${}^3\text{He}$ effective-range parameters will be presented.

A. The CHH Method

In the CHH approach a four-nucleon wave function Ψ is expanded as

$$\Psi = \sum_p \left[\psi_A(\mathbf{x}_{Ap}, \mathbf{y}_{Ap}, \mathbf{z}_{Ap}) + \psi_B(\mathbf{x}_{Bp}, \mathbf{y}_{Bp}, \mathbf{z}_{Bp}) \right], \quad (3.1)$$

where the amplitudes ψ_A and ψ_B correspond, respectively, to the partitions 3+1 and 2+2, and the index p runs over the even permutations of particles $ijkl$. The dependence on the spin-isospin variables is understood. The overall antisymmetry of the wave function Ψ is ensured by requiring that both ψ_A and ψ_B change sign under the exchange $i \rightleftharpoons j$.

The Jacobi variables corresponding to the partition 3+1 are defined as

$$\mathbf{x}_{Ap} = \mathbf{r}_j - \mathbf{r}_i, \quad (3.2)$$

$$\mathbf{y}_{Ap} = \sqrt{4/3}(\mathbf{r}_k - \mathbf{R}_{ij}), \quad (3.3)$$

$$\mathbf{z}_{Ap} = \sqrt{3/2}(\mathbf{r}_l - \mathbf{R}_{ijk}), \quad (3.4)$$

while those corresponding to the partition 2+2 are defined as

$$\mathbf{x}_{Bp} = \mathbf{r}_j - \mathbf{r}_i , \quad (3.5)$$

$$\mathbf{y}_{Bp} = \sqrt{2}(\mathbf{R}_{kl} - \mathbf{R}_{ij}) , \quad (3.6)$$

$$\mathbf{z}_{Bp} = \mathbf{r}_l - \mathbf{r}_k , \quad (3.7)$$

where \mathbf{R}_{ij} (\mathbf{R}_{kl}) and \mathbf{R}_{ijk} denote the c.m. positions of particles ij (kl) and ijk , respectively. In the LS -coupling scheme, the amplitudes ψ_A and ψ_B are expanded as

$$\psi_A(\mathbf{x}_{Ap}, \mathbf{y}_{Ap}, \mathbf{z}_{Ap}) = \sum_{\alpha} F_{\alpha,p} \phi_{\alpha}^A(x_{Ap}, y_{Ap}, z_{Ap}) Y_{\alpha,p}^A , \quad (3.8)$$

$$\psi_B(\mathbf{x}_{Bp}, \mathbf{y}_{Bp}, \mathbf{z}_{Bp}) = \sum_{\alpha} F_{\alpha,p} \phi_{\alpha}^B(x_{Bp}, y_{Bp}, z_{Bp}) Y_{\alpha,p}^B , \quad (3.9)$$

where

$$Y_{\alpha,p}^A = \left\{ \left[[Y_{\ell_{1\alpha}}(\hat{\mathbf{z}}_{Ap}) Y_{\ell_{2\alpha}}(\hat{\mathbf{y}}_{Ap})]_{\ell_{12\alpha}} Y_{\ell_{3\alpha}}(\hat{\mathbf{x}}_{Ap}) \right]_{L_{\alpha}} \left[\left[[s_i s_j]_{S_{a\alpha}} s_k \right]_{S_{b\alpha}} s_l \right]_{S_{\alpha}} \right\}_{JJ_z} \\ \times \left[[t_i t_j]_{T_{a\alpha}} t_k \right]_{T_{b\alpha}} t_l \Big|_{TT_z} , \quad (3.10)$$

$$Y_{\alpha,p}^B = \left\{ \left[[Y_{\ell_{1\alpha}}(\hat{\mathbf{z}}_{Bp}) Y_{\ell_{2\alpha}}(\hat{\mathbf{y}}_{Bp})]_{\ell_{12\alpha}} Y_{\ell_{3\alpha}}(\hat{\mathbf{x}}_{Bp}) \right]_{L_{\alpha}} \left[[s_i s_j]_{S_{a\alpha}} [s_k s_l]_{S_{b\alpha}} \right]_{S_{\alpha}} \right\}_{JJ_z} \\ \times \left[[t_i t_j]_{T_{a\alpha}} [t_k t_l]_{T_{b\alpha}} \right]_{TT_z} . \quad (3.11)$$

Here a channel α is specified by: orbital angular momenta $\ell_{1\alpha}$, $\ell_{2\alpha}$, $\ell_{3\alpha}$, $\ell_{12\alpha}$, and L_{α} ; spin angular momenta $S_{a\alpha}$, $S_{b\alpha}$, and S_{α} ; isospins $T_{a\alpha}$ and $T_{b\alpha}$. The total orbital and spin angular momenta and cluster isospins are then coupled to the assigned JJ_z and TT_z .

The correlation factors $F_{\alpha,p}$ consist of the product of pair-correlation functions, that are obtained from solutions of two-body Schrödinger-like equations, as discussed in Ref. [34]. These correlation factors take into account the strong state-dependent correlations induced by the nucleon-nucleon interaction, and improve the behavior of the wave function at small interparticle separations, thus accelerating the convergence of the calculated quantities with respect to the number of required hyperspherical harmonics basis functions, defined below.

The radial amplitudes ϕ_{α}^A and ϕ_{α}^B are further expanded as

$$\phi_{\alpha}^A(x_{Ap}, y_{Ap}, z_{Ap}) = \sum_{n,m} \frac{u_{nm}^{\alpha}(\rho)}{\rho^4} z_{Ap}^{\ell_{1\alpha}} y_{Ap}^{\ell_{2\alpha}} x_{Ap}^{\ell_{3\alpha}} X_{nm}^{\alpha}(\phi_{2p}^A, \phi_{3p}^A) , \quad (3.12)$$

$$\phi_{\alpha}^B(x_{Bp}, y_{Bp}, z_{Bp}) = \sum_{n,m} \frac{w_{nm}^{\alpha}(\rho)}{\rho^4} z_{Bp}^{\ell_{1\alpha}} y_{Bp}^{\ell_{2\alpha}} x_{Bp}^{\ell_{3\alpha}} X_{nm}^{\alpha}(\phi_{2p}^B, \phi_{3p}^B) , \quad (3.13)$$

where the magnitudes of the Jacobi variables have been replaced by the hyperspherical coordinates, i.e. the hyperradius ρ

$$\rho = \sqrt{x_{Ap}^2 + y_{Ap}^2 + z_{Ap}^2} = \sqrt{x_{Bp}^2 + y_{Bp}^2 + z_{Bp}^2}, \quad (3.14)$$

which is independent of the permutation p considered, and the hyperangles appropriate for partitions A and B . The latter are given by

$$\cos \phi_{3p} = x_{Ap}/\rho = x_{Bp}/\rho, \quad (3.15)$$

$$\cos \phi_{2p}^A = y_{Ap}/(\rho \sin \phi_{3p}), \quad (3.16)$$

$$\cos \phi_{2p}^B = y_{Bp}/(\rho \sin \phi_{3p}). \quad (3.17)$$

Finally, the hyperangle functions X_{nm}^α consist of the product of Jacobi polynomials

$$X_{nm}^\alpha(\beta, \gamma) = N_{nm}^\alpha (\sin \beta)^{2m} P_n^{K_{2\alpha}, \ell_{3\alpha} + \frac{1}{2}}(\cos 2\beta) P_m^{\ell_{1\alpha} + \frac{1}{2}, \ell_{2\alpha} + \frac{1}{2}}(\cos 2\gamma), \quad (3.18)$$

where the indices m and n run, in principle, over all non-negative integers, $K_{2\alpha} = \ell_{1\alpha} + \ell_{2\alpha} + 2m + 2$, and N_{nm}^α are normalization factors [34].

Once the expansions for the radial amplitudes ϕ^A and ϕ^B are inserted into Eqs. (3.8)–(3.9), the wave function Ψ can schematically be written as

$$\Psi = \sum_{\alpha nm} \left[\frac{z_{nm}^{\alpha,A}(\rho)}{\rho^4} Z_{nm}^{\alpha,A}(\rho, \Omega) + \frac{z_{nm}^{\alpha,B}(\rho)}{\rho^4} Z_{nm}^{\alpha,B}(\rho, \Omega) \right], \quad (3.19)$$

where $z^A(\rho) \equiv u(\rho)$ and $z^B(\rho) \equiv w(\rho)$ are yet to be determined, and the factors $Z_{nm}^{\alpha,W}$, with $W = A, B$, include the dependence upon the hyperradius ρ due to the correlation functions, and the angles and hyperangles, denoted collectively by Ω , and are given by:

$$Z_{nm}^{\alpha,W}(\rho, \Omega) = \sum_p F_{\alpha,p} Y_{\alpha,p}^W z_{W,p}^{\ell_{1\alpha}} y_{W,p}^{\ell_{2\alpha}} x_{W,p}^{\ell_{3\alpha}} X_{n,m}^\alpha(\phi_{2p}^W, \phi_{3p}^W). \quad (3.20)$$

The CHH method for three-nucleon systems has been most recently reviewed in Ref. [18], and will not be discussed here. It leads, in essence, to wave functions having the same structure as in Eq. (3.19) with suitably defined $Z(\rho, \Omega)$.

B. The ${}^3\text{He}$ and ${}^4\text{He}$ Wave Functions

The Rayleigh-Ritz variational principle

$$\langle \delta_z \Psi | H - E | \Psi \rangle = 0 \quad (3.21)$$

is used to determine the hyperradial functions $z_{nm}^\alpha(\rho)$ in Eq. (3.19) and bound state energy E . Carrying out the variations with respect to the functions z_{nm}^α leads to a set of coupled second-order linear differential equations in the variable ρ which, after discretization, is converted into a generalized eigenvalue problem and solved by standard numerical techniques [34].

The present status of ${}^3\text{He}$ [58] and ${}^4\text{He}$ [34,36] binding energy calculations with the CHH method is summarized in Tables II and III. The binding energies calculated with the CHH method using the AV18 or AV18/UIX Hamiltonian models are within 1.5 % of corresponding “exact” Green’s function Monte Carlo (GFMC) results [32], and of the experimental value (when the three-nucleon interaction is included). The agreement between the CHH and GFMC results is less satisfactory when the AV14 or AV14/UVIII models are considered, presumably because of slower convergence of the CHH expansions for the AV14 interaction. This interaction has tensor components which do not vanish at the origin.

C. The $p^3\text{He}$ Continuum Wave Functions

The $p^3\text{He}$ cluster wave function $\Psi_{1+3}^{LSJJ_z}$, having incoming orbital angular momentum L and channel spin S ($S = 0, 1$) coupled to total angular JJ_z , is expressed as

$$\Psi_{1+3}^{LSJJ_z} = \Psi_C^{JJ_z} + \Psi_A^{LSJJ_z}, \quad (3.22)$$

where the term Ψ_C vanishes in the limit of large intercluster separations, and hence describes the system in the region where the particles are close to each other and their mutual interactions are strong. The term $\Psi_A^{LSJJ_z}$ describes the system in the asymptotic region, where intercluster interactions are negligible. It is given explicitly as:

$$\begin{aligned} \Psi_A^{LSJJ_z} = & \frac{1}{\sqrt{4}} \sum_i \sum_{L'S'} [[s_i \otimes \phi_3(jkl)]_{S'} \otimes Y_{L'}(\hat{\mathbf{y}}_i)]_{JJ_z} \\ & \times \left[\delta_{LL'} \delta_{SS'} \frac{F_{L'}(py_i)}{py_i} + R_{LS,L'S'}^J(p) \frac{G_{L'}(py_i)}{py_i} g(y_i) \right], \end{aligned} \quad (3.23)$$

where y_i is the distance between the proton (particle i) and ^3He (particles jkl), p is the magnitude of the relative momentum between the two clusters, ϕ_3 is the ^3He wave function, and F_L and G_L are the regular and irregular Coulomb functions, respectively. The function $g(y_i)$ modifies the $G_L(py_i)$ at small y_i by regularizing it at the origin, and $g(y_i) \rightarrow 1$ as $y_i \gtrsim 10$ fm, thus not affecting the asymptotic behavior of $\Psi_{1+3}^{LSJJ_z}$. Finally, the real parameters $R_{LS,L'S'}^J(p)$ are the R -matrix elements introduced in Eq. (2.6), which determine phase shifts and (for coupled channels) mixing angles at the energy $p^2/(2\mu)$ (μ is $p^3\text{He}$ reduced mass). Of course, the sum over L' and S' is over all values compatible with a given J and parity.

The ‘‘core’’ wave function Ψ_C is expanded in the same CHH basis as the bound-state wave function, and both the matrix elements $R_{LS,L'S'}^J(p)$ and functions $z_{nm}^\alpha(\rho)$ occurring in the expansion of Ψ_C are determined by making the functional

$$[R_{LS,L'S'}^J(p)] = R_{LS,L'S'}^J(p) - \frac{m}{\sqrt{6}} \langle \Psi_{1+3}^{L'S'JJ_z} | H - E_3 - \frac{p^2}{2\mu} | \Psi_{1+3}^{LSJJ_z} \rangle, \quad (3.24)$$

stationary with respect to variations in the $R_{LS,L'S'}^J$ and z_{nm}^α (Kohn variational principle). Here $E_3 = -7.72$ MeV is the ^3He ground-state energy. It is important to emphasize that the CHH scheme, in contrast to Faddeev-Yakubovsky momentum space methods, permits the straightforward inclusion of Coulomb distortion effects in the $p^3\text{He}$ channel.

The $p^3\text{He}$ singlet and triplet scattering lengths predicted by the Hamiltonian models considered in the present work are listed in Table III, and are found in good agreement with available experimental values, although these are rather poorly known. The experimental scattering lengths have been obtained, in fact, from effective range parametrizations of data taken above 1 MeV, and therefore might have large systematic uncertainties.

The most recent determination of phase-shift and mixing-angle parameters for $p^3\text{He}$ elastic scattering has been performed in Ref. [41] by means of an energy-dependent phase-shift analysis (PSA), including almost all data measured prior 1993 (for a listing of old PSAs, see Ref. [41]). New measurements are currently under way at TUNL [59] and Madison [60]. At low energies ($E < 4$ MeV) the process is dominated by scattering in $L=0$ and 1 waves, with a small contribution from $L=2$ waves. Therefore, the important channels are: $^1\text{S}_0$,

3P_0 , 3S_1 - 3D_1 , 1P_1 - 3P_1 , 3P_2 , 1D_2 - 3D_2 and 3D_3 , ignoring channels with $L > 2$. The general trend is the following: (i) the energy dependence of the S-wave phase shifts indicates that the $L=0$ channel interaction between the p and ${}^3\text{He}$ is repulsive (mostly, due to the Pauli principle), while that of the four P-wave phase shifts (3P_0 , 1P_1 , 3P_1 , and 3P_2) shows that in these channels there is a strong attraction. Indeed, this fact has led to speculations about the existence of four resonant states [61]. (ii) The D-wave phase shifts are rather tiny, even at $E > 2$ MeV. (iii) The only mixing-angle parameter playing an important role at $E < 4$ MeV is $\epsilon(J^\pi = 1^-)$, in channel 1P_1 - 3P_1 .

Precise measurements have been taken at a c.m. energy of 1.2 MeV, and consist in differential cross section $\sigma(\theta)$ [62] and proton analyzing power $A_y(\theta)$ [60] data (θ is the c.m. scattering angle). The theoretical predictions for $\sigma(\theta)$, obtained from the AV18 and AV18/UIX interactions, are compared with the corresponding experimental data in Fig. 2. Inspection of the figure shows that the differential cross section calculated with the AV18/UIX model is in excellent agreement with the data, except at backward angles.

By comparing, in Table IV, the calculated phase-shift and mixing-angle parameters with those extracted from the PSA [41] at $E = 1.2$ MeV, one observes a qualitative agreement, except for the 3P_1 and 3P_2 phase shifts which are significantly underestimated in the calculation. The mixing-angle parameter $\epsilon(1^-)$ is found to be rather large, $\simeq -14^\circ$, in qualitative agreement with that obtained from the PSA (it is worth pointing out, however, that in the PSA the mixing angle was constrained to vanish at $E = 0$, which may be unphysical). The experimental error for each parameter quoted in Ref. [41] is an average uncertainty over the whole energy range considered, and it is therefore only indicative. It would be very interesting to relate these discrepancies to the $Nd A_y$ puzzle and to specific deficiencies in the nuclear interaction models. A detailed study of p - ${}^3\text{He}$ elastic scattering is currently underway and will be published elsewhere [63].

IV. THE WEAK CHARGE AND CURRENT OPERATORS

The nuclear weak charge and current operators have scalar/polar-vector (V) and pseudoscalar/axial-vector (A) components

$$\rho_\pm(\mathbf{q}) = \rho_\pm(\mathbf{q}; V) + \rho_\pm(\mathbf{q}; A) , \quad (4.1)$$

$$\mathbf{j}_\pm(\mathbf{q}) = \mathbf{j}_\pm(\mathbf{q}; V) + \mathbf{j}_\pm(\mathbf{q}; A) , \quad (4.2)$$

where \mathbf{q} is the momentum transfer, $\mathbf{q} = \mathbf{p}_e + \mathbf{p}_\nu$, and the subscripts \pm denote charge raising (+) or lowering (-) isospin indices. Each component, in turn, consists of one-, two-, and many-body terms that operate on the nucleon degrees of freedom:

$$\rho(\mathbf{q}; a) = \sum_i \rho_i^{(1)}(\mathbf{q}; a) + \sum_{i < j} \rho_{ij}^{(2)}(\mathbf{q}; a) + \dots , \quad (4.3)$$

$$\mathbf{j}(\mathbf{q}; a) = \sum_i \mathbf{j}_i^{(1)}(\mathbf{q}; a) + \sum_{i < j} \mathbf{j}_{ij}^{(2)}(\mathbf{q}; a) + \dots , \quad (4.4)$$

where $a=V, A$ and the isospin indices have been suppressed to simplify the notation. The one-body operators $\rho_i^{(1)}$ and $\mathbf{j}_i^{(1)}$ have the standard expressions obtained from a non-relativistic reduction of the covariant single-nucleon V and A currents, and are listed below for convenience. The V-charge operator is written as

$$\rho_i^{(1)}(\mathbf{q}; V) = \rho_{i,\text{NR}}^{(1)}(\mathbf{q}; V) + \rho_{i,\text{RC}}^{(1)}(\mathbf{q}; V) , \quad (4.5)$$

with

$$\rho_{i,\text{NR}}^{(1)}(\mathbf{q}; V) = \tau_{i,\pm} e^{i\mathbf{q}\cdot\mathbf{r}_i} , \quad (4.6)$$

$$\rho_{i,\text{RC}}^{(1)}(\mathbf{q}; V) = -i \frac{(2\mu^v - 1)}{4m^2} \tau_{i,\pm} \mathbf{q} \cdot (\boldsymbol{\sigma}_i \times \mathbf{p}_i) e^{i\mathbf{q}\cdot\mathbf{r}_i} . \quad (4.7)$$

The V-current operator is expressed as

$$\mathbf{j}_i^{(1)}(\mathbf{q}; V) = \frac{1}{2m} \tau_{i,\pm} \left[\mathbf{p}_i , e^{i\mathbf{q}\cdot\mathbf{r}_i} \right]_+ - i \frac{\mu^v}{2m} \tau_{i,\pm} \mathbf{q} \times \boldsymbol{\sigma}_i e^{i\mathbf{q}\cdot\mathbf{r}_i} , \quad (4.8)$$

where $[\dots, \dots]_+$ denotes the anticommutator, \mathbf{p} , $\boldsymbol{\sigma}$, and $\boldsymbol{\tau}$ are the nucleon's momentum, Pauli spin and isospin operators, respectively, and μ^v is the isovector nucleon magnetic moment ($\mu^v = 4.709$ n.m.). Finally, the isospin raising and lowering operators are defined as

$$\tau_{i,\pm} \equiv (\tau_{i,x} \pm i\tau_{i,y})/2 . \quad (4.9)$$

The term proportional to $1/m^2$ in $\rho_{i,\text{RC}}^{(1)}(\mathbf{q}; V)$ is the well known [64,65] spin-orbit relativistic correction. The vector charge and current operators above are simply obtained from the corresponding isovector electromagnetic operators by the replacement $\tau_{i,z}/2 \rightarrow \tau_{i,\pm}$, in accordance with the conserved-vector-current (CVC) hypothesis. The q -dependence of the nucleon's vector form factors (and, in fact, also that of the axial-vector form factors below) has been ignored, since the weak transition under consideration here involves very small momentum transfers, $q \leq 20$ MeV/c. For this same reason, the Darwin-Foldy relativistic correction proportional to $q^2/(8m^2)$ in $\rho_{i,\text{RC}}^{(1)}(\mathbf{q}; V)$ has also been neglected. The A-charge operator is given, to leading order, by

$$\rho_i^{(1)}(\mathbf{q}; A) = -\frac{g_A}{2m} \tau_{i,\pm} \boldsymbol{\sigma}_i \cdot \left[\mathbf{p}_i , e^{i\mathbf{q}\cdot\mathbf{r}_i} \right]_+ , \quad (4.10)$$

while the A-current operator considered in the present work includes leading and next-to-leading order corrections in an expansion in powers of p/m , i.e.

$$\mathbf{j}_i^{(1)}(\mathbf{q}; A) = \mathbf{j}_{i,\text{NR}}^{(1)}(\mathbf{q}; A) + \mathbf{j}_{i,\text{RC}}^{(1)}(\mathbf{q}; A) , \quad (4.11)$$

with

$$\mathbf{j}_{i,\text{NR}}^{(1)}(\mathbf{q}; A) = -g_A \tau_{i,\pm} \boldsymbol{\sigma}_i e^{i\mathbf{q}\cdot\mathbf{r}_i} , \quad (4.12)$$

$$\begin{aligned} \mathbf{j}_{i,\text{RC}}^{(1)}(\mathbf{q}; A) = & \frac{g_A}{4m^2} \tau_{i,\pm} \left(\boldsymbol{\sigma}_i \left[\mathbf{p}_i^2 , e^{i\mathbf{q}\cdot\mathbf{r}_i} \right]_+ - \left[\boldsymbol{\sigma}_i \cdot \mathbf{p}_i \mathbf{p}_i , e^{i\mathbf{q}\cdot\mathbf{r}_i} \right]_+ - \frac{1}{2} \boldsymbol{\sigma}_i \cdot \mathbf{q} \left[\mathbf{p}_i , e^{i\mathbf{q}\cdot\mathbf{r}_i} \right]_+ \right. \\ & \left. - \frac{1}{2} \mathbf{q} \left[\boldsymbol{\sigma}_i \cdot \mathbf{p}_i , e^{i\mathbf{q}\cdot\mathbf{r}_i} \right]_+ + i \mathbf{q} \times \mathbf{p}_i e^{i\mathbf{q}\cdot\mathbf{r}_i} \right) - \frac{g_P}{2m m_\mu} \tau_{i,\pm} \mathbf{q} \boldsymbol{\sigma}_i \cdot \mathbf{q} e^{i\mathbf{q}\cdot\mathbf{r}_i} . \end{aligned} \quad (4.13)$$

The axial coupling constant g_A is taken to be [66] 1.2654 ± 0.0042 , by averaging values obtained, respectively, from the beta asymmetry in the decay of polarized neutrons (1.2626 ± 0.0033 [67,68]) and the half-lives of the neutron and superallowed $0^+ \rightarrow 0^+$ transitions, i.e. $[2ft(0^+ \rightarrow 0^+)/ft(n) - 1] = 1.2681 \pm 0.0033$ [66]. The last term in Eq. (4.13) is the induced pseudoscalar contribution (m_μ is the muon mass), for which the coupling constant g_P is taken as [69] $g_P = -6.78 g_A$. As already mentioned in Sec. I, in 3S_1 capture matrix elements of $\mathbf{j}_{i,\text{NR}}^{(1)}$ are suppressed. Consequently, the relativistic terms included in $\mathbf{j}_{i,\text{RC}}^{(1)}$, which would otherwise contribute at the percent level, give in fact a 20 % contribution relative to that of the leading $\mathbf{j}_{i,\text{NR}}^{(1)}$ at $q=0$. Among these, one would naively expect the induced pseudoscalar term to be dominant, due to the relatively large value of g_P . This is not the case, however, since matrix elements of the induced pseudoscalar term scale with $g_P q^2 / (2g_A m m_\mu)$ (≤ 0.014 in the q -range of interest) relative to those $\hat{\mathbf{q}} \cdot \mathbf{j}_{i,\text{NR}}^{(1)}(\mathbf{q}; A)$. Note that in the limit $q=0$, the expressions for $\rho_{i,\text{NR}}^{(1)}(\mathbf{q}; V)$ and $\mathbf{j}_{i,\text{NR}}^{(1)}(\mathbf{q}; A)$ reduce to the familiar Fermi and Gamow-Teller operators.

In the next five subsections we describe: i) the two-body V-current and V-charge operators, required by the CVC hypothesis; ii) the two-body A-current and A-charge operators due to π - and ρ -meson exchanges, and the $\rho\pi$ mechanism; iii) the V and A current and charge operators associated with excitation of Δ -isobar resonances, treated in perturbation theory and within the transition-correlation-operator method. Since the expressions for these operators are scattered in a number of papers [11,20,70,71], we collect them here for completeness.

A. Two-Body Weak Vector Current Operators

The weak vector (V) current and charge operators are derived from the corresponding electromagnetic operators by making use of the CVC hypothesis, which for two-body terms implies

$$\left[\frac{1}{2}(\tau_{i,a} + \tau_{j,a}), \mathbf{j}_{ij,z}^{(2)}(\mathbf{q}; \gamma) \right] = i \epsilon_{azb} \mathbf{j}_{ij,b}^{(2)}(\mathbf{q}; V), \quad (4.14)$$

where $\mathbf{j}_{ij,z}^{(2)}(\mathbf{q}; \gamma)$ are the isovector (charge-conserving) two-body electromagnetic currents, and $a, b = x, y, z$ are isospin Cartesian components. A similar relation holds between the electromagnetic charge operators and its weak vector counterparts. The charge-raising or lowering weak vector current (or charge) operators are then simply obtained from the linear combinations

$$\mathbf{j}_{ij,\pm}^{(2)}(\mathbf{q}; V) = \mathbf{j}_{ij,x}^{(2)}(\mathbf{q}; V) \pm i \mathbf{j}_{ij,y}^{(2)}(\mathbf{q}; V). \quad (4.15)$$

The two-body electromagnetic currents have “model-independent” (MI) and “model-dependent” (MD) components, in the classification scheme of Riska [72]. The MI terms are obtained from the two-nucleon interaction, and by construction satisfy current conservation with it [70]. Studies of the electromagnetic structure of $A=2-6$ nuclei, such as, for example, the threshold electrodisintegration of the deuteron at backward angles [73], the magnetic form factors of the trinucleons [42], the magnetic dipole transition form factors

in ${}^6\text{Li}$ [74], and finally the neutron and proton radiative captures on hydrogen and helium isotopes [19,73,75]—properties in which the isovector two-body currents play a large role and are, in fact, essential for the satisfactory description of the experimental data—have shown that the leading operator is the (isovector) “ π -like” current obtained from the isospin-dependent spin-spin and tensor interactions. The latter also generate an isovector “ ρ -like” current. There are additional MI isovector currents, which arise from the central and momentum-dependent interactions, but these are short-ranged and have been found to be numerically far less important than the π -like current [70,73]. Their contributions are neglected in the present study.

Use of the CVC relation leads to the π -like and ρ -like weak vector currents below:

$$\begin{aligned} \mathbf{j}_{ij}^{(2)}(\mathbf{k}_i, \mathbf{k}_j; \pi V) = & i(\boldsymbol{\tau}_i \times \boldsymbol{\tau}_j)_\pm \left[v_{PS}(k_j) \boldsymbol{\sigma}_i (\boldsymbol{\sigma}_j \cdot \mathbf{k}_j) - v_{PS}(k_i) \boldsymbol{\sigma}_j (\boldsymbol{\sigma}_i \cdot \mathbf{k}_i) \right. \\ & \left. + \frac{\mathbf{k}_i - \mathbf{k}_j}{k_i^2 - k_j^2} [v_{PS}(k_i) - v_{PS}(k_j)] (\boldsymbol{\sigma}_i \cdot \mathbf{k}_i) (\boldsymbol{\sigma}_j \cdot \mathbf{k}_j) \right] , \end{aligned} \quad (4.16)$$

$$\begin{aligned} \mathbf{j}_{ij}^{(2)}(\mathbf{k}_i, \mathbf{k}_j; \rho V) = & -i(\boldsymbol{\tau}_i \times \boldsymbol{\tau}_j)_\pm \left[v_V(k_j) \boldsymbol{\sigma}_i \times (\boldsymbol{\sigma}_j \times \mathbf{k}_j) - v_V(k_i) \boldsymbol{\sigma}_j \times (\boldsymbol{\sigma}_i \times \mathbf{k}_i) \right. \\ & - \frac{v_V(k_i) - v_V(k_j)}{k_i^2 - k_j^2} [(\mathbf{k}_i - \mathbf{k}_j) (\boldsymbol{\sigma}_i \times \mathbf{k}_i) \cdot (\boldsymbol{\sigma}_j \times \mathbf{k}_j) \\ & + (\boldsymbol{\sigma}_i \times \mathbf{k}_i) \boldsymbol{\sigma}_j \cdot (\mathbf{k}_i \times \mathbf{k}_j) + (\boldsymbol{\sigma}_j \times \mathbf{k}_j) \boldsymbol{\sigma}_i \cdot (\mathbf{k}_i \times \mathbf{k}_j)] \\ & \left. + \frac{\mathbf{k}_i - \mathbf{k}_j}{k_i^2 - k_j^2} [v_{VS}(k_i) - v_{VS}(k_j)] \right] , \end{aligned} \quad (4.17)$$

where \mathbf{k}_i and \mathbf{k}_j are the momenta delivered to nucleons i and j with $\mathbf{q} = \mathbf{k}_i + \mathbf{k}_j$, the isospin operators are defined as

$$(\boldsymbol{\tau}_i \times \boldsymbol{\tau}_j)_\pm \equiv (\boldsymbol{\tau}_i \times \boldsymbol{\tau}_j)_x \pm i(\boldsymbol{\tau}_i \times \boldsymbol{\tau}_j)_y , \quad (4.18)$$

and $v_{PS}(k)$, $v_V(k)$, and $v_{VS}(k)$ are given by

$$v_{PS}(k) = v^{\sigma\tau}(k) - 2v^{t\tau}(k) , \quad (4.19)$$

$$v_V(k) = v^{\sigma\tau}(k) + v^{t\tau}(k) , \quad (4.20)$$

$$v_{VS}(k) = v^\tau(k) , \quad (4.21)$$

with

$$v^\tau(k) = 4\pi \int_0^\infty r^2 dr j_0(kr) v^\tau(r) , \quad (4.22)$$

$$v^{\sigma\tau}(k) = \frac{4\pi}{k^2} \int_0^\infty r^2 dr [j_0(kr) - 1] v^{\sigma\tau}(r) , \quad (4.23)$$

$$v^{t\tau}(k) = \frac{4\pi}{k^2} \int_0^\infty r^2 dr j_2(kr) v^{t\tau}(r) . \quad (4.24)$$

Here $v^\tau(r)$, $v^{\sigma\tau}(r)$, $v^{t\tau}(r)$ are the isospin-dependent central, spin-spin, and tensor components of the two-nucleon interaction (either the AV14 or AV18 in the present study). The

factor $j_0(kr) - 1$ in the expression for $v^{\sigma\tau}(k)$ ensures that its volume integral vanishes. Configuration-space expressions are obtained from

$$\mathbf{j}_{ij}^{(2)}(\mathbf{q}; \mathbf{a}) = \int d\mathbf{x} e^{i\mathbf{q}\cdot\mathbf{x}} \int \frac{d\mathbf{k}_i}{(2\pi)^3} \frac{d\mathbf{k}_j}{(2\pi)^3} e^{i\mathbf{k}_i\cdot(\mathbf{r}_i-\mathbf{x})} e^{i\mathbf{k}_j\cdot(\mathbf{r}_j-\mathbf{x})} \mathbf{j}_{ij}^{(2)}(\mathbf{k}_i, \mathbf{k}_j; \mathbf{a}) , \quad (4.25)$$

where $\mathbf{a}=\pi\mathbf{V}$ or $\rho\mathbf{V}$. Techniques to carry out the Fourier transforms above are discussed in Ref. [70].

In a one-boson-exchange (OBE) model, in which the isospin-dependent central, spin-spin, and tensor interactions are due to π - and ρ -meson exchanges, the functions $v_{PS}(k)$, $v_V(k)$, and $v_{VS}(k)$ are simply given by

$$v_{PS}(k) \rightarrow v_\pi(k) \equiv -\frac{f_\pi^2}{m_\pi^2} \frac{f_\pi^2(k)}{k^2 + m_\pi^2} , \quad (4.26)$$

$$v_V(k) \rightarrow v_\rho(k) \equiv -\frac{g_\rho^2(1 + \kappa_\rho)^2}{4m^2} \frac{f_\rho^2(k)}{k^2 + m_\rho^2} , \quad (4.27)$$

$$v_{VS}(k) \rightarrow v_{\rho S} \equiv g_\rho^2 \frac{f_\rho^2(k)}{k^2 + m_\rho^2} , \quad (4.28)$$

where m_π and m_ρ are the meson masses, f_π , g_ρ and κ_ρ are the pseudovector πNN , vector and tensor ρNN coupling constants, respectively, $f_\pi(k)$ and $f_\rho(k)$ denote πNN and ρNN monopole form factors, i.e.

$$f_\alpha(k) = \frac{\Lambda_\alpha^2 - m_\alpha^2}{\Lambda_\alpha^2 + k^2} , \quad (4.29)$$

with $\alpha=\pi$ or ρ . For example, in the CD-Bonn OBE model [46] the values for the couplings and cutoff masses are: $f_\pi^2/4\pi = 0.075$, $g_\rho^2/4\pi = 0.84$, $k_\rho = 6.1$, $\Lambda_\pi = 1.7$ GeV/c, and $\Lambda_\rho = 1.31$ GeV/c. Even though the AV14 and AV18 are not OBE models, the functions $v_{PS}(k)$ and, to a less extent, $v_V(k)$ and $v_{VS}(k)$ projected out from their v^τ , $v^{\sigma\tau}$, and $v^{t\tau}$ components are quite similar to those of π - and ρ -meson exchanges in Eqs. (4.26)–(4.28) (with cutoff masses of order 1 GeV/c), as shown in Refs. [70,75].

Among the MD (purely transverse) isovector currents, those due to excitation of Δ isobars have been found to be the most important, particularly at low momentum transfers, in studies of electromagnetic structure [42] and reactions [11] of few-nucleon systems. Their contribution, however, is still relatively small when compared to that of the leading π -like current. Discussion of the weak vector currents associated with Δ degrees of freedom is deferred to Sec. IV E.

B. Two-Body Weak Vector Charge Operators

While the main parts of the two-body electromagnetic or weak vector current are linked to the form of the nucleon-nucleon interaction through the continuity equation, the most important two-body electromagnetic or weak vector charge operators are model dependent, and should be viewed as relativistic corrections. Indeed, a consistent calculation of two-body charge effects in nuclei would require the inclusion of relativistic effects in both the

interaction models and nuclear wave functions. Such a program is yet to be carried out, at least for systems with $A \geq 3$.

There are nevertheless rather clear indications for the relevance of two-body electromagnetic charge operators from the failure of the impulse approximation in predicting the deuteron tensor polarization observable [76], and charge form factors of the three- and four-nucleon systems [42,77]. The model commonly used [71] includes the π -, ρ -, and ω -meson exchange charge operators with both isoscalar and isovector components, as well as the (isoscalar) $\rho\pi\gamma$ and (isovector) $\omega\pi\gamma$ charge transition couplings (in addition to the single-nucleon Darwin-Foldy and spin-orbit relativistic corrections). The π - and ρ -meson exchange charge operators are constructed from the isospin-dependent spin-spin and tensor interactions, using the same prescription adopted for the corresponding current operators [71]. At moderate values of momentum transfer ($q < 5 \text{ fm}^{-1}$), the contribution due to the “ π -like” exchange charge operator has been found to be typically an order of magnitude larger than that of any of the remaining two-body mechanisms and one-body relativistic corrections [42].

In the present study we retain, in addition to the one-body operator of Eq. (4.5), only the “ π -like” and “ ρ -like” weak vector charge operators. In the notation of the previous subsection, these are given by

$$\rho_{ij}^{(2)}(\mathbf{k}_i, \mathbf{k}_j; \pi V) = -\frac{1}{m} \left[\tau_{j,\pm} v_{PS}(k_j) \boldsymbol{\sigma}_i \cdot \mathbf{q} \boldsymbol{\sigma}_j \cdot \mathbf{k}_j + \tau_{i,\pm} v_{PS}(k_i) \boldsymbol{\sigma}_i \cdot \mathbf{k}_i \boldsymbol{\sigma}_j \cdot \mathbf{q} \right], \quad (4.30)$$

$$\begin{aligned} \rho_{ij}^{(2)}(\mathbf{k}_i, \mathbf{k}_j; \rho V) = & -\frac{1}{m} \left[\tau_{j,\pm} v_V(k_j) (\boldsymbol{\sigma}_i \times \mathbf{q}) \cdot (\boldsymbol{\sigma}_j \times \mathbf{k}_j) \right. \\ & \left. + \tau_{i,\pm} v_V(k_i) (\boldsymbol{\sigma}_j \times \mathbf{q}) \cdot (\boldsymbol{\sigma}_i \times \mathbf{k}_i) \right], \end{aligned} \quad (4.31)$$

where non-local terms from retardation effects in the meson propagators or from direct couplings to the exchanged mesons have been neglected [78,79]. In the $\rho_{ij}^{(2)}(\mathbf{k}_i, \mathbf{k}_j; \rho V)$ operator terms proportional to powers of $1/(1 + \kappa_\rho)$, because of the large ρ -meson tensor coupling ($\kappa_\rho \simeq 6-7$), have also been neglected. Indeed, these terms have been ignored also in most studies of nuclear charge form factors.

C. Two-Body Weak Axial Current Operators

In contrast to the electromagnetic case, the axial current operator is not conserved. Its two-body components cannot be linked to the nucleon-nucleon interaction and, in this sense, should be viewed as model dependent. Among the two-body axial current operators, the leading term is that associated with excitation of Δ -isobar resonances. We again defer its discussion to Sec. IV E. In the present section we list the two-body axial current operators due to π - and ρ -meson exchanges (the πA and ρA currents, respectively), and the $\rho\pi$ -transition mechanism (the $\rho\pi A$ current). Their individual contributions have been found numerically far less important than those from Δ -excitation currents in studies of weak transitions involving light nuclei [20,45,80]. These studies [20,45] have also found that the

πA and ρA current contributions interfere destructively, making their combined contribution almost entirely negligible. These conclusions are confirmed in the present work.

The πA , ρA , and $\rho\pi A$ current operators were first described in a systematic way by Chemtob and Rho [21]. Their derivation has been given in a number of articles, including the original reference mentioned above and the more recent review by Towner [22]. Their momentum-space expressions are given by

$$\begin{aligned} \mathbf{j}_{ij}^{(2)}(\mathbf{k}_i, \mathbf{k}_j; \pi A) = & -\frac{g_A}{2m} (\boldsymbol{\tau}_i \times \boldsymbol{\tau}_j)_\pm v_\pi(k_j) \boldsymbol{\sigma}_i \times \mathbf{k}_j \boldsymbol{\sigma}_j \cdot \mathbf{k}_j \\ & + \frac{g_A}{m} \tau_{j,\pm} v_\pi(k_j) (\mathbf{q} + i \boldsymbol{\sigma}_i \times \mathbf{P}_i) \boldsymbol{\sigma}_j \cdot \mathbf{k}_j + i \rightleftharpoons j, \end{aligned} \quad (4.32)$$

$$\begin{aligned} \mathbf{j}_{ij}^{(2)}(\mathbf{k}_i, \mathbf{k}_j; \rho A) = & \frac{g_A}{2m} (\boldsymbol{\tau}_i \times \boldsymbol{\tau}_j)_\pm v_\rho(k_j) \left[\mathbf{q} \boldsymbol{\sigma}_i \cdot (\boldsymbol{\sigma}_j \times \mathbf{k}_j) + i(\boldsymbol{\sigma}_j \times \mathbf{k}_j) \times \mathbf{P}_i \right. \\ & \left. - [\boldsymbol{\sigma}_i \times (\boldsymbol{\sigma}_j \times \mathbf{k}_j)] \times \mathbf{k}_j \right] \\ & + \frac{g_A}{m} \tau_{j,\pm} v_\rho(k_j) \left[(\boldsymbol{\sigma}_j \times \mathbf{k}_j) \times \mathbf{k}_j - i[\boldsymbol{\sigma}_i \times (\boldsymbol{\sigma}_j \times \mathbf{k}_j)] \times \mathbf{P}_i \right] + i \rightleftharpoons j, \end{aligned} \quad (4.33)$$

$$\begin{aligned} \mathbf{j}_{ij}^{(2)}(\mathbf{k}_i, \mathbf{k}_j; \rho\pi A) = & -\frac{g_A}{m} g_\rho^2 (\boldsymbol{\tau}_i \times \boldsymbol{\tau}_j)_\pm \frac{f_\rho(k_i)}{k_i^2 + m_\rho^2} \frac{f_\pi(k_j)}{k_j^2 + m_\pi^2} \boldsymbol{\sigma}_j \cdot \mathbf{k}_j \\ & \times \left[(1 + \kappa_\rho) \boldsymbol{\sigma}_i \times \mathbf{k}_i - i \mathbf{P}_i \right] + i \rightleftharpoons j, \end{aligned} \quad (4.34)$$

where $\mathbf{P}_i = \mathbf{p}_i + \mathbf{p}'_i$ is the sum of the initial and final momenta of nucleon i , respectively \mathbf{p}_i and \mathbf{p}'_i , and the functions $v_\pi(k)$ and $v_\rho(k)$ have already been defined in Eqs. (4.26)–(4.27). Configuration-space expressions are obtained by carrying out the Fourier transforms in Eq. (4.25). The values used for the πNN and ρNN coupling constants and cutoff masses are the following: $f_\pi^2/4\pi = 0.075$, $g_\rho^2/4\pi = 0.5$, $\kappa_\rho = 6.6$, $\Lambda_\pi = 4.8 \text{ fm}^{-1}$, and $\Lambda_\rho = 6.8 \text{ fm}^{-1}$. The ρ -meson coupling constants are taken from the older Bonn OBE model [81], rather than from the more recent CD-Bonn interaction [46] ($g_\rho^2/4\pi = 0.81$ and $\kappa_\rho = 6.1$). This uncertainty has in fact essentially no impact on the results reported in the present work for two reasons. Firstly, the contribution from $\mathbf{j}^{(2)}(\rho A)$, as already mentioned above, is very small. Secondly, the complete two-body axial current model, including the currents due to Δ -excitation discussed below, is constrained to reproduce the Gamow-Teller matrix element in tritium β -decay by appropriately tuning the value of the $N\Delta$ -transition axial coupling g_A^* . Hence changes in g_ρ and κ_ρ only require a slight readjustment of the g_A^* value.

Finally, note that the replacements $v_\pi(k) \rightarrow v_{PS}(k)$ and $v_\rho(k) \rightarrow v_V(k)$ could have been made in the expressions for $\mathbf{j}^{(2)}(\pi A)$ and $\mathbf{j}^{(2)}(\rho A)$ above, thus eliminating the need for the inclusion of *ad hoc* form factors. While this procedure would have been more satisfactory, since it constrains the short-range behavior of these currents in a way consistent with that of the two-nucleon interaction, its impact on the present calculations would still be marginal for the same reasons given above.

D. Two-Body Weak Axial Charge Operators

The model for the weak axial charge operator adopted here includes a term of pion-range as well as short-range terms associated with scalar- and vector-meson exchanges [44]. The

experimental evidence for the presence of these two-body axial charge mechanisms rests on studies of $0^+ \rightleftharpoons 0^-$ weak transitions, such as the processes $^{16}\text{N}(0^-, 120 \text{ keV}) \rightarrow ^{16}\text{O}(0^+)$ and $^{16}\text{O}(0^+) + \mu^- \rightarrow ^{16}\text{N}(0^-, 120 \text{ keV}) + \nu_\mu$, and first-forbidden β -decays in the lead region [82]. Shell-model calculations of these transitions suggest that the effective axial charge coupling of a bound nucleon may be enhanced by roughly a factor of two over its free nucleon value. There are rather strong indications that such an enhancement can be explained by two-body axial charge contributions [44].

The pion-range operator is taken as

$$\rho_{ij}^{(2)}(\mathbf{k}_i, \mathbf{k}_j; \pi A) = -i \frac{g_A}{4 \bar{f}_\pi^2} (\boldsymbol{\tau}_i \times \boldsymbol{\tau}_j)_\pm \frac{f_\pi^2(k_i)}{k_i^2 + m_\pi^2} \boldsymbol{\sigma}_i \cdot \mathbf{k}_i + i \rightleftharpoons j, \quad (4.35)$$

where \bar{f}_π is the pion decay constant ($\bar{f}_\pi = 93 \text{ MeV}$), \mathbf{k}_i is the momentum transfer to nucleon i , and $f_\pi(k)$ is the monopole form factor of Eq. (4.29) with $\Lambda_\pi = 4.8 \text{ fm}^{-1}$. The structure and overall strength of this operator are determined by soft pion theorem and current algebra arguments [43,83], and should therefore be viewed as “model independent”. It can also be derived, however, by considering nucleon-antinucleon pair contributions with pseudoscalar πN coupling.

The short-range axial charge operators can be obtained in a “model-independent” way, consistently with the two-nucleon interaction model. The procedure is described in Ref. [44], and is similar to the one used to derive the “model-independent” electromagnetic or weak vector currents. Here we consider the charge operators associated only with the central and spin-orbit components of the interaction, since these are expected to give the largest contributions, after the $\rho^{(2)}(\pi A)$ operator above. This expectation is in fact confirmed in the present study. The momentum-space expressions are given by

$$\rho_{ij}^{(2)}(\mathbf{k}_i, \mathbf{k}_j; sA) = \frac{g_A}{2m^2} [\tau_{i,\pm} \bar{v}^s(k_j) + \tau_{j,\pm} \bar{v}^{s\tau}(k_j)] \boldsymbol{\sigma}_i \cdot \mathbf{P}_i + i \rightleftharpoons j, \quad (4.36)$$

$$\begin{aligned} \rho_{ij}^{(2)}(\mathbf{k}_i, \mathbf{k}_j; vA) &= \frac{g_A}{2m^2} [\tau_{i,\pm} \bar{v}^v(k_j) + \tau_{j,\pm} \bar{v}^{v\tau}(k_j)] [\boldsymbol{\sigma}_i \cdot \mathbf{P}_j + i (\boldsymbol{\sigma}_i \times \boldsymbol{\sigma}_j) \cdot \mathbf{k}_j] \\ &\quad - i \frac{g_A}{4m^2} (\boldsymbol{\tau}_i \times \boldsymbol{\tau}_j)_\pm \bar{v}^{v\tau}(k_j) \boldsymbol{\sigma}_i \cdot \mathbf{k}_i + i \rightleftharpoons j, \end{aligned} \quad (4.37)$$

where $\mathbf{P}_i = \mathbf{p}_i + \mathbf{p}'_i$, and

$$\bar{v}^\alpha(k) = 4\pi \int_0^\infty dr r^2 j_0(kr) \bar{v}^\alpha(r), \quad (4.38)$$

with $\alpha = s, s\tau, v$, and $v\tau$. The following definitions have been introduced

$$\begin{aligned} \bar{v}^s(r) &= \frac{3}{4} v^c(r) + \frac{m^2}{2} \int_r^\infty dr' r' \left[v^b(r') - \frac{1}{2} v^{bb}(r') \right] \\ \bar{v}^v(r) &= \frac{1}{4} v^c(r) - \frac{m^2}{2} \int_r^\infty dr' r' \left[v^b(r') - \frac{1}{2} v^{bb}(r') \right], \end{aligned} \quad (4.39)$$

where $v^c(r)$, $v^b(r)$ and $v^{bb}(r)$ are the isospin-independent central, spin-orbit, and $(\mathbf{L} \cdot \mathbf{S})^2$ components of the AV14 or AV18 interactions, respectively. The definitions for $\bar{v}^{s\tau}(r)$ and $\bar{v}^{v\tau}(r)$ can be obtained from those above, by replacing the isospin-independent $v^c(r)$, $v^b(r)$ and $v^{bb}(r)$ with the isospin-dependent $v^{c\tau}(r)$, $v^{b\tau}(r)$ and $v^{bb\tau}(r)$.

E. Δ -Isobar Contributions

In this section we review the treatment of the weak current and charge operators associated with excitation of Δ isobars in perturbation theory and within the context of the transition-correlation-operator (TCO) method [11]. Among the two-body axial current operators, those associated with Δ degrees of freedom have in fact been found to be the most important ones [11,20].

In the TCO approach, the nuclear wave function is written as

$$\Psi_{N+\Delta} = \left[\mathcal{S} \prod_{i<j} (1 + U_{ij}^{\text{TR}}) \right] \Psi, \quad (4.40)$$

where Ψ is the purely nucleonic component, \mathcal{S} is the symmetrizer, and the transition operators U_{ij}^{TR} convert NN pairs into $N\Delta$ and $\Delta\Delta$ pairs. The latter are defined as

$$U_{ij}^{\text{TR}} = U_{ij}^{N\Delta} + U_{ij}^{\Delta N} + U_{ij}^{\Delta\Delta}, \quad (4.41)$$

$$U_{ij}^{N\Delta} = [u^{\sigma\tau II}(r_{ij})\boldsymbol{\sigma}_i \cdot \mathbf{S}_j + u^{t\tau II}(r_{ij})S_{ij}^{II}] \boldsymbol{\tau}_i \cdot \mathbf{T}_j, \quad (4.42)$$

$$U_{ij}^{\Delta\Delta} = [u^{\sigma\tau III}(r_{ij})\mathbf{S}_i \cdot \mathbf{S}_j + u^{t\tau III}(r_{ij})S_{ij}^{III}] \mathbf{T}_i \cdot \mathbf{T}_j. \quad (4.43)$$

Here, \mathbf{S}_i and \mathbf{T}_i are spin- and isospin-transition operators which convert nucleon i into a Δ isobar, S_{ij}^{II} and S_{ij}^{III} are tensor operators in which, respectively, the Pauli spin operators of either particle i or j , and both particles i and j are replaced by corresponding spin-transition operators. The U_{ij}^{TR} vanishes in the limit of large interparticle separations, since no Δ -components can exist asymptotically.

In the present study the Ψ is taken from CHH solutions of the AV14/UVIII or AV18/UIX Hamiltonians with nucleons only interactions, while the U_{ij}^{TR} is obtained from two-body bound and low-energy scattering-state solutions of the full N - Δ coupled-channel problem with the Argonne v_{28Q} [84] (AV28Q) interaction, containing explicit N and Δ degrees of freedom. This aspect of the present calculations, including the validity of the approximation inherent to Eq. (4.40), were discussed at length in the original work [11], and have been reviewed more recently in Ref. [42], making a further review here unnecessary. The AV28Q interaction provided an excellent description of the NN database available in the early eighties. No attempt has been made to refit this model to the more recent and much more extensive Nijmegen database [85].

In the TCO scheme, the perturbation theory description of Δ -admixture is equivalent to the replacements:

$$U_{ij}^{N\Delta, \text{PT}} = \frac{v_{ij}(NN \rightarrow N\Delta)}{m - m_\Delta}, \quad (4.44)$$

$$U_{ij}^{\Delta\Delta, \text{PT}} = \frac{v_{ij}(NN \rightarrow \Delta\Delta)}{2(m - m_\Delta)}, \quad (4.45)$$

where the kinetic energy contributions in the denominators of Eqs. (4.44) and (4.45) have been neglected (static Δ approximation). The transition interactions $v_{ij}(NN \rightarrow N\Delta)$ and

$v_{ij}(NN \rightarrow \Delta\Delta)$ have the same operator structure as $U_{ij}^{N\Delta}$ and $U_{ij}^{\Delta\Delta}$ of Eqs. (4.42) and (4.43), but with the $u^{\sigma\tau\alpha}(r)$ and $u^{t\tau\alpha}(r)$ functions replaced by v_{ij} , respectively,

$$v^{\sigma\tau\alpha}(r) = \frac{(ff)_\alpha m_\pi e^{-x}}{4\pi \frac{3}{x}} C(x) , \quad (4.46)$$

$$v^{t\tau\alpha}(r) = \frac{(ff)_\alpha m_\pi}{4\pi \frac{3}{x}} \left(1 + \frac{3}{x} + \frac{3}{x^2} \right) \frac{e^{-x}}{x} C^2(x) . \quad (4.47)$$

Here $\alpha = \text{II, III}$, $x \equiv m_\pi r$, $(ff)_\alpha = f_\pi f_\pi^*$, $f_\pi^* f_\pi$ for $\alpha = \text{II, III}$, respectively, f_π^* being the $\pi N\Delta$ coupling constant, and the cutoff function $C(x) = 1 - e^{-\lambda x^2}$. In the AV28Q interaction $f_\pi^* = (6\sqrt{2}/5)f_\pi$, as obtained in the quark-model, and $\lambda = 4.09$. When compared to U_{ij}^{TR} , the perturbation theory $U_{ij}^{\text{TR,PT}}$ corresponding to Eqs. (4.44) and (4.45) produces $N\Delta$ and $\Delta\Delta$ admixtures that are too large at short distances, and therefore leads to a substantial overprediction of the effects associated with Δ isobars in electroweak observables [11].

We now turn our attention to the discussion of $N\Delta$ and $\Delta\Delta$ weak transition operators. The axial current and charge operators associated with excitation of Δ isobars are modeled as

$$\mathbf{j}_i^{(1)}(\mathbf{q}; N \rightarrow \Delta, A) = -g_A^* T_{i,\pm} \mathbf{S}_i e^{i\mathbf{q}\cdot\mathbf{r}_i} , \quad (4.48)$$

$$\mathbf{j}_i^{(1)}(\mathbf{q}; \Delta \rightarrow \Delta, A) = -\bar{g}_A \Theta_{i,\pm} \boldsymbol{\Sigma}_i e^{i\mathbf{q}\cdot\mathbf{r}_i} , \quad (4.49)$$

and

$$\rho_i^{(1)}(\mathbf{q}; N \rightarrow \Delta, A) = -\frac{g_A^*}{m_\Delta} T_{i,\pm} \mathbf{S}_i \cdot \mathbf{p}_i e^{i\mathbf{q}\cdot\mathbf{r}_i} \quad (4.50)$$

$$\rho_i^{(1)}(\mathbf{q}; \Delta \rightarrow \Delta, A) = -\frac{\bar{g}_A}{2m_\Delta} \Theta_{i,\pm} \boldsymbol{\Sigma}_i \cdot \left[\mathbf{p}_i, e^{i\mathbf{q}\cdot\mathbf{r}_i} \right]_+ , \quad (4.51)$$

where m_Δ is the Δ -isobar mass, $\boldsymbol{\Sigma}$ ($\boldsymbol{\Theta}$) is the Pauli operator for the Δ spin 3/2 (isospin 3/2), and $T_{i,\pm}$ and $\Theta_{i,\pm}$ are defined in analogy to Eq. (4.9). The expression for $\mathbf{j}_i^{(1)}(\mathbf{q}; \Delta \rightarrow N, A)$ ($\rho_i^{(1)}(\mathbf{q}; \Delta \rightarrow N, A)$) is obtained from that for $\mathbf{j}_i^{(1)}(\mathbf{q}; N \rightarrow \Delta, A)$ ($\rho_i^{(1)}(\mathbf{q}; N \rightarrow \Delta, A)$) by replacing \mathbf{S}_i and \mathbf{T}_i by their hermitian conjugates. The coupling constants g_A^* and \bar{g}_A are not well known. In the quark-model, they are related to the axial coupling constant of the nucleon by the relations $g_A^* = (6\sqrt{2}/5)g_A$ and $\bar{g}_A = (1/5)g_A$. These values have often been used in the literature in the calculation of Δ -induced axial current contributions to weak transitions. However, given the uncertainties inherent to quark-model predictions, a more reliable estimate for g_A^* is obtained by determining its value phenomenologically in the following way. It is well established by now [45] that the one-body axial current of Eq. (4.12) leads to a $\simeq 4$ % underprediction of the measured Gamow-Teller matrix element in tritium β -decay, see Table V. Since the contributions of $\Delta \rightarrow \Delta$ axial currents (as well as those due to the two-body operators of Sec. IV C) are found to be numerically very small, as can be seen again from Table V, this 4 % discrepancy can then be used to determine g_A^* [86]. Obviously, this procedure produces different values for g_A^* depending on how the Δ -isobar degrees of freedom are treated. These values are listed in Table VI for comparison. The g_A^* value that is determined in the context of a TCO calculation based on the AV28Q interaction, is about 40 % larger than the naive quark-model estimate. However, when perturbation theory is used for the treatment of the Δ isobars, the g_A^* value required to reproduce the

Gamow-Teller matrix element of tritium β -decay is much smaller than the TCO estimate, as expected. Finally, the $N \rightarrow \Delta$ axial current derived in perturbation theory from Eqs. (4.44) and (4.48) is, of course, identical to the expression given in Refs. [20,45].

The $N \rightarrow \Delta$ and $\Delta \rightarrow \Delta$ weak vector currents are modeled, consistently with the CVC hypothesis, as

$$\mathbf{j}_i^{(1)}(\mathbf{q}; N \rightarrow \Delta, V) = -i \frac{\mu^*}{m} T_{i,\pm} \mathbf{q} \times \mathbf{S}_i e^{i\mathbf{q}\cdot\mathbf{r}_i} , \quad (4.52)$$

$$\mathbf{j}_i^{(1)}(\mathbf{q}; \Delta \rightarrow \Delta, V) = -i \frac{\bar{\mu}}{12m} \Theta_{i,\pm} \mathbf{q} \times \boldsymbol{\Sigma}_i e^{i\mathbf{q}\cdot\mathbf{r}_i} , \quad (4.53)$$

where the $N\Delta$ -transition magnetic moment μ^* is taken equal to 3 n.m., as obtained from an analysis of γN data in the Δ -resonance region [87], while the value used for the Δ magnetic moment $\bar{\mu}$ is 4.35 n.m. by averaging results of a soft-photon analysis of pion-proton bremsstrahlung data near the Δ^{++} resonance [88]. The contributions due to the weak vector currents above have been in fact found to be very small in the $p^3\text{He}$ capture process. Finally, Δ to Δ weak vector charge operators are ignored in the present study, since their associated contributions are expected to be negligible.

V. CALCULATION

The calculation of the $p^3\text{He}$ weak capture cross section proceeds in two steps: firstly, the Monte Carlo evaluation of the weak charge and current operator matrix elements, and the subsequent decomposition of these in terms of reduced matrix elements; secondly, the evaluation of the cross section by carrying out the integrations in Eq. (2.22).

A. Monte Carlo Calculation of Matrix Elements

In a frame where the direction of the momentum transfer $\hat{\mathbf{q}}$ also defines the quantization axis of the nuclear spins, the matrix element of, as an example, the weak axial (or vector) current has the multipole expansion

$$\langle \Psi_4 | \hat{\mathbf{e}}_{q\lambda}^* \cdot \mathbf{j}^\dagger(\mathbf{q}) | \bar{\Psi}_{1+3}^{LSJ, J_z=\lambda} \rangle = \sqrt{2\pi} i^J [\lambda M_J^{LSJ}(q) + E_J^{LSJ}(q)] , \quad (5.1)$$

with $\lambda = \pm 1$. The expansion above is easily obtained from that in Eq. (2.16), in which the quantization axis for the nuclear spins was taken along the direction of the relative momentum $\hat{\mathbf{p}}$, by setting $\theta=\phi=0$ and using $D_{J'_z, J_z}^J(0, 0, 0) = \delta_{J'_z, J_z}$. Then, again as an example, the reduced matrix element of the axial electric dipole operator involving a transition from the $p^3\text{He } ^3\text{S}_1$ state is simply given by

$$E_1^{011}(q; A) = -\frac{i}{\sqrt{2\pi}} \langle \Psi_4 | \hat{\mathbf{e}}_{q\lambda}^* \cdot \mathbf{j}^\dagger(\mathbf{q}; A) | \bar{\Psi}_{1+3}^{011, J_z=\lambda} \rangle . \quad (5.2)$$

The problem is now reduced to the evaluation of matrix elements of the same type as on the right-hand-side of Eq. (5.2). These can schematically be written as

$$\frac{\langle \Psi_{4,N+\Delta} | O | \Psi_{1+3,N+\Delta} \rangle}{[\langle \Psi_{4,N+\Delta} | \Psi_{4,N+\Delta} \rangle \langle \Psi_{1+3,N+\Delta} | \Psi_{1+3,N+\Delta} \rangle]^{1/2}}, \quad (5.3)$$

where the initial and final states have the form of Eq. (4.40). It is convenient to expand the latter as

$$\Psi_{N+\Delta} = \Psi + \sum_{i < j} U_{ij}^{\text{TR}} \Psi + \dots, \quad (5.4)$$

so that the numerator of Eq. (5.3) can be expressed as

$$\langle \Psi_{4,N+\Delta} | O | \Psi_{1+3,N+\Delta} \rangle = \langle \Psi_4 | O(N \text{ only}) | \Psi_{1+3} \rangle + \langle \Psi_4 | O(\Delta) | \Psi_{1+3} \rangle, \quad (5.5)$$

where the operator $O(N \text{ only})$ denotes all one- and two-body contributions to the weak charge or current operator O , involving only nucleon degrees of freedom, i.e. $O(N \text{ only}) = O^{(1)}(N \rightarrow N) + O^{(2)}(NN \rightarrow NN)$, while $O(\Delta)$ includes terms that involve the Δ -isobar degrees of freedom, associated with the explicit Δ transitions $O^{(1)}(N \rightarrow \Delta)$, $O^{(1)}(\Delta \rightarrow N)$, $O^{(1)}(\Delta \rightarrow \Delta)$, and with the transition operators U_{ij}^{TR} . A diagrammatical illustration of the terms contributing to $O(\Delta)$ is given in Fig. 3: the terms (a)–(e), (f)–(i), and (j) represent, respectively, two-, three-, and four-body operators. The terms (e) and (g)–(j) are to be viewed as renormalization corrections to the “nucleonic” matrix element of $O^{(1)}(N \rightarrow N)$, due to the presence of Δ -admixture in the wave functions. Connected three-body terms containing more than a single Δ isobar have been ignored, since their contributions are expected to be negligible. Indeed, the contribution from diagram (d) has already been found numerically very small.

The two-body terms of Fig. 3 are expanded as operators acting on the nucleons’ coordinates. For example, the terms (a) and (c) in Fig. 3 have the structure, respectively,

$$(a) = U_{ij}^{\Delta N \dagger} O_i^{(1)}(N \rightarrow \Delta), \quad (5.6)$$

$$(c) = U_{ij}^{\Delta N \dagger} O_i^{(1)}(\Delta \rightarrow \Delta) U_{ij}^{\Delta N}, \quad (5.7)$$

which can be reduced to operators involving only Pauli spin and isospin matrices by using the identities:

$$\mathbf{S}^\dagger \cdot \mathbf{A} \mathbf{S} \cdot \mathbf{B} = \frac{2}{3} \mathbf{A} \cdot \mathbf{B} - \frac{i}{3} \boldsymbol{\sigma} \cdot (\mathbf{A} \times \mathbf{B}), \quad (5.8)$$

$$\begin{aligned} \mathbf{S}^\dagger \cdot \mathbf{A} \boldsymbol{\Sigma} \cdot \mathbf{B} \mathbf{S} \cdot \mathbf{C} &= \frac{5}{3} i \mathbf{A} \cdot (\mathbf{B} \times \mathbf{C}) - \frac{1}{3} \boldsymbol{\sigma} \cdot \mathbf{A} \mathbf{B} \cdot \mathbf{C} \\ &\quad - \frac{1}{3} \mathbf{A} \cdot \mathbf{B} \mathbf{C} \cdot \boldsymbol{\sigma} + \frac{4}{3} \mathbf{A} \cdot (\mathbf{B} \cdot \boldsymbol{\sigma}) \mathbf{C}, \end{aligned} \quad (5.9)$$

where \mathbf{A} , \mathbf{B} and \mathbf{C} are vector operators that commute with $\boldsymbol{\sigma}$, but not necessarily among themselves. While the three- and four-body terms in Fig. 3 could have been reduced in precisely the same way, the resulting expressions in terms of $\boldsymbol{\sigma}$ and $\boldsymbol{\tau}$ matrices become too cumbersome. Thus, for these it was found to be more convenient to retain the explicit representation of \mathbf{S} (\mathbf{S}^\dagger) as a 4×2 (2×4) matrix

$$\mathbf{S} = \begin{bmatrix} -\hat{\mathbf{e}}_- & 0 \\ \sqrt{\frac{2}{3}}\hat{\mathbf{e}}_0 & -\frac{1}{\sqrt{3}}\hat{\mathbf{e}}_- \\ -\frac{1}{\sqrt{3}}\hat{\mathbf{e}}_+ & \sqrt{\frac{2}{3}}\hat{\mathbf{e}}_0 \\ 0 & -\hat{\mathbf{e}}_+ \end{bmatrix},$$

and of Σ as a 4×4 matrix

$$\Sigma = \begin{bmatrix} 3\hat{\mathbf{e}}_0 & \sqrt{6}\hat{\mathbf{e}}_- & 0 & 0 \\ -\sqrt{6}\hat{\mathbf{e}}_+ & \hat{\mathbf{e}}_0 & \sqrt{8}\hat{\mathbf{e}}_- & 0 \\ 0 & -\sqrt{8}\hat{\mathbf{e}}_+ & -\hat{\mathbf{e}}_0 & \sqrt{6}\hat{\mathbf{e}}_- \\ 0 & 0 & -\sqrt{6}\hat{\mathbf{e}}_+ & -3\hat{\mathbf{e}}_0 \end{bmatrix},$$

where $\hat{\mathbf{e}}_{\pm} = \mp(\hat{\mathbf{x}} \pm i\hat{\mathbf{y}})/\sqrt{2}$, $\hat{\mathbf{e}}_0 = \hat{\mathbf{z}}$, and $\hat{\mathbf{e}}_{\mu}^* = (-)^{\mu}\hat{\mathbf{e}}_{-\mu}$, and derive the result of terms such as $(f) = U_{ij}^{N\Delta\dagger} O_j^{(1)}(\Delta \rightarrow \Delta) U_{jk}^{\Delta N}$ on state $|\Psi\rangle$ by first operating with $U_{jk}^{\Delta N}$, then with $O_j^{(1)}(\Delta \rightarrow \Delta)$, and finally with $U_{ij}^{N\Delta\dagger}$. These terms (as well as three-body contributions to the wave function normalizations, see below) were neglected in the calculations reported in Ref. [11].

Of course, the presence of Δ -admixture also influences the normalization of the wave functions, as is obvious from Eq. (5.3):

$$\begin{aligned} \langle \Psi_{N+\Delta} | \Psi_{N+\Delta} \rangle &= \langle \Psi | 1 + \sum_{i<j} [2U_{ij}^{\Delta N\dagger} U_{ij}^{\Delta N} + U_{ij}^{\Delta\Delta\dagger} U_{ij}^{\Delta\Delta}] \\ &+ \sum_{i<j, k \neq i, j} [U_{ij}^{\Delta N\dagger} U_{ik}^{\Delta N} + U_{ij}^{N\Delta\dagger} U_{kj}^{N\Delta}] | \Psi \rangle + \dots \end{aligned} \quad (5.10)$$

The wave function normalization ratios $\langle \Psi_{N+\Delta} | \Psi_{N+\Delta} \rangle / \langle \Psi | \Psi \rangle$, obtained for the bound three- and four-nucleon systems, are listed in Table VII. Note that the normalization of the $p^3\text{He}$ continuum state is the same as that of ^3He , up to corrections of order $(\text{volume})^{-1}$.

The matrix elements in Eqs. (5.5) and (5.10) are computed, without any approximation, by Monte Carlo integrations. The wave functions are written as vectors in the spin-isospin space of the four nucleons for any given spatial configuration $\mathbf{R} = (\mathbf{r}_1, \dots, \mathbf{r}_4)$. For the given \mathbf{R} we calculate the state vector $[O(\mathbf{R}, N \text{ only}) + O(\mathbf{R}, \Delta)] \Psi(\mathbf{R})$ with the techniques developed in Refs. [42,70]. The spatial integrations are carried out with the Monte Carlo method by sampling \mathbf{R} configurations according to the Metropolis *et al.* algorithm [89], using a probability density $W(\mathbf{R})$ proportional to

$$W(\mathbf{R}) \propto \sqrt{\langle \Psi_4^\dagger(\mathbf{R}) \Psi_4(\mathbf{R}) \rangle}, \quad (5.11)$$

where the notation $\langle \dots \rangle$ implies sums over the spin-isospin states of the ^4He wave function. Typically 200,000 configurations are enough to achieve a relative error $\leq 5\%$ on the total S -factor.

B. Calculation of Cross Section

Once the reduced matrix elements (RMEs) have been obtained, the calculation of the cross section $\sigma(E)$ is reduced to performing the integrations over the electron and neutrino momenta in Eq. (2.22) numerically. We write

$$\sigma(E) = \frac{1}{(2\pi)^2} \frac{G_V^2}{v_{\text{rel}}} \int_0^{p_e^*} dp_e p_e^2 \int_{-1}^1 dx_e \int_{-1}^1 dx_\nu \int_0^{2\pi} d\phi p_\nu^2 f^{-1} L_{\sigma\tau} N^{\sigma\tau}, \quad (5.12)$$

where one of the azimuthal integrations has been carried out, since the integrand only depends on the difference $\phi = \phi_e - \phi_\nu$. The δ -function occurring in Eq. (2.22) has also been integrated out resulting in the factor f^{-1} , with

$$f = \left| 1 + \frac{p_e x_{e\nu}}{m_4} + \frac{p_\nu}{m_4} \right|. \quad (5.13)$$

The magnitude of the neutrino momentum is fixed by energy conservation to be

$$p_\nu = \frac{2\bar{\Delta}}{1 + p_e x_{e\nu}/m_4 + \sqrt{(1 + p_e x_{e\nu}/m_4)^2 + 2\bar{\Delta}/m_4}}, \quad (5.14)$$

where $\bar{\Delta} = \Delta m + E - E_e - p_e^2/2m_4$. The variable $x_{e\nu}$ is defined as

$$x_{e\nu} = \hat{\mathbf{p}}_e \cdot \hat{\mathbf{p}}_\nu = x_e x_\nu + \sqrt{1 - x_e^2} \sqrt{1 - x_\nu^2} \cos \phi, \quad (5.15)$$

where $x_e = \cos \theta_e$ and $x_\nu = \cos \theta_\nu$. Finally, the integration over the magnitude of the electron momentum extends from zero up to

$$p_e^* = \sqrt{\left[\sqrt{m_4^2 + m_e^2 + 2m_4(\Delta m + E)} - m_4^2 \right]^2 - m_e^2}. \quad (5.16)$$

The lepton tensor is explicitly given by Eq. (2.24), while the nuclear tensor is constructed using Eqs. (2.25)–(2.29). Computer codes have been developed to calculate the required rotation matrices corresponding to the $\hat{\mathbf{q}}$ -direction (θ, ϕ) with

$$\begin{aligned} \cos \theta &= \hat{\mathbf{z}} \cdot \hat{\mathbf{q}} = \frac{\hat{\mathbf{z}} \cdot (\mathbf{p}_e + \mathbf{p}_\nu)}{|\mathbf{p}_e + \mathbf{p}_\nu|} \\ &= \frac{p_e x_e + p_\nu x_\nu}{\sqrt{p_e^2 + p_\nu^2 + 2p_e p_\nu x_{e\nu}}}. \end{aligned} \quad (5.17)$$

Finally, note that the nuclear tensor requires the values of the RMEs at the momentum transfer q (the denominator in the second line of Eq. (5.17)). It has been found convenient to make the dependence upon q of the RMEs explicit by expanding

$$T_J^{LSJ}(q) = q^m \sum_{n \geq 0} t_{2n}^{LSJ} q^{2n}, \quad (5.18)$$

consistently with Eqs. (2.17)–(2.20). Here $m = J, J \pm 1$, depending on the RME considered. For example, $m = 1$ for the $L_0^{110}(\text{A})$ RME. Given the low momentum transfers involved, $q \leq 20$ MeV/c, the leading and next-to-leading order terms t_0 and t_2 are sufficient to reproduce accurately $T(q)$. Note that the long-wavelength-approximation corresponds, typically, to retaining only the t_0 term.

A moderate number of Gauss points (of the order of 10) for each of the integrations in Eq. (5.12) is sufficient to achieve convergence within better than one part in 10^3 . The computer program has been successfully tested by reproducing the result obtained analytically by retaining only the ${}^3\text{S}_1 E_1(\text{A})$ and $L_1(\text{A})$ and ${}^3\text{P}_0 C_0(\text{A})$ RMEs.

VI. RESULTS AND DISCUSSION

The S -factor calculated values are listed in Table I, and their implications to the recoil electron spectrum measured in the SK experiment, see Fig. 1, have already been discussed in the introduction. In Tables VIII, IX, and XII-XV, we present our results, obtained with the AV18/UIX Hamiltonian model, for the reduced matrix elements (RMEs) connecting any of the $p^3\text{He}$ S- and P-wave channels to the ^4He bound state. The values for these RMEs are given at zero energy and a lepton momentum transfer $q=19.2$ MeV/c. Note that the RMEs listed in all tables are related to those defined in Eqs. (2.14)–(2.16) via

$$\overline{T}_J^{LSJ} = \sqrt{\frac{v_{\text{rel}}}{4\pi\alpha} [\exp(4\pi\alpha/v_{\text{rel}}) - 1]} T_J^{LSJ} , \quad (6.1)$$

which can be shown to remain finite in the limit $v_{\text{rel}} \rightarrow 0$, corresponding to zero energy.

In Table XVI we list the individual contributions of the S- and P-wave capture channels to the total S -factor at zero c.m. energy, obtained with the AV18/UIX, the AV18 only (to study the effects of the three-nucleon interaction), and the older AV14/UVIII (to study the model dependence and to make contact with the earlier calculations of Refs. [11,20]). The model dependence is discussed in Sec. VID.

In Tables I, VIII, IX, and XI-XV, the cumulative nucleonic contributions are normalized as

$$[\text{one-body} + \text{mesonic}] = \frac{\langle \Psi_4 | O(N \text{ only}) | \Psi_{1+3} \rangle}{[\langle \Psi_4 | \Psi_4 \rangle \langle \Psi_{1+3} | \Psi_{1+3} \rangle]^{1/2}} . \quad (6.2)$$

However, when the Δ -isobar contributions are added to the cumulative sum, the normalization changes to

$$[\text{one-body} + \text{mesonic} + \Delta] = \frac{\langle \Psi_{4,N+\Delta} | O(N \text{ only}) + O(\Delta) | \Psi_{1+3,N+\Delta} \rangle}{[\langle \Psi_{4,N+\Delta} | \Psi_{4,N+\Delta} \rangle \langle \Psi_{1+3,N+\Delta} | \Psi_{1+3,N+\Delta} \rangle]^{1/2}} . \quad (6.3)$$

As already pointed out earlier in Sec. VA, the normalization of the initial scattering state is the same as that of ^3He , up to corrections of order (volume) $^{-1}$. In Table XI we also report results in which the Δ -components in the nuclear wave functions are treated in perturbation theory, as discussed in Secs. IVE and VA, and the $O(\Delta)$ only includes the operators in panel (a) of Fig. 3. In this case, the cumulative contributions [one-body+mesonic+ Δ_{PT}] are normalized as in Eq. (6.2).

A. $^1\text{S}_0$ Capture

The $^1\text{S}_0$ capture is induced by the weak vector charge and longitudinal component of the weak vector current via the $C_0(V)$ and $L_0(V)$ multipoles, respectively. The associated RMEs, while small, are not negligible—they are about 20 % of the “large” $E_1(A)$ RME in $^3\text{S}_1$ capture, see Table IX. These $^1\text{S}_0$ transitions are inhibited by an isospin selection rule, indeed they vanish at $q=0$, since in this limit

$$C_0(q; V) \rightarrow \frac{1}{\sqrt{4\pi}} \sum_i \tau_{i,\pm} \equiv \frac{1}{\sqrt{4\pi}} T_{\pm} , \quad (6.4)$$

and

$$L_0(q; V) = -\frac{1}{q} \left[H, \int d\mathbf{x} j_0(qx) Y_{00}(\hat{\mathbf{x}}) \rho(\mathbf{x}; V) \right] \rightarrow -\frac{1}{q} \left[H, \frac{1}{\sqrt{4\pi}} T_{\pm} \right], \quad (6.5)$$

where the expression for $L_0(V)$ has been obtained by integrating Eq. (2.18) by parts, and then using the continuity equation to relate $\nabla \cdot \mathbf{j}(\mathbf{x}; V)$ to the commutator $-i[H, \rho(\mathbf{x}; V)]$. The ${}^4\text{He}$ and p ${}^3\text{He}$ states have total isospins $T, T_z=0,0$ and $1,1$, respectively, ignoring additional, but very small, isospin admixtures induced by isospin-symmetry-breaking components of the interaction. Therefore matrix elements of the (total) isospin raising or lowering operators T_{\pm} between these T, T_z states vanish.

Equation (6.5) shows that, if the initial and final CHH wave functions were to be exact eigenfunctions of the AV18/UIX Hamiltonian, then one would expect, neglecting the kinetic energy of the recoiling ${}^4\text{He}$:

$$L_0(q; V) = \frac{E_3 - E_4}{q} C_0(q; V), \quad (6.6)$$

where E_3 and E_4 are the three- and four-nucleon ground-state energies. Note that the relation above is in fact valid for any $C_J(q; V)$ and $L_J(q; V)$ multipoles. For $q=19.2$ MeV/c the ratio L_0/C_0 is expected to be 1.07, which is in perfect agreement with that obtained in the calculation, when the two-body current contributions are taken into account, see Table VIII. As already discussed in Sec. IV A, the present model for the weak vector current satisfies current conservation with the v_6 part of the nucleon-nucleon interaction (either AV14 or AV18). The spin-orbit and quadratic momentum-dependent components of the interaction, however, require additional short-range currents that have been neglected in this work. If their contributions were to be completely negligible, then the degree of agreement between the expected and calculated values for the ratio L_0/C_0 would simply reflect the extent to which the present variational wave functions are truly exact eigenfunctions of the AV18/UIX Hamiltonian. However, the CHH wave function used here gives a ground-state energy of -27.9 MeV for ${}^4\text{He}$, which is about 400 keV higher than predicted for the AV18/UIX model in GFMC calculations [32]. In view of these considerations, the perfect agreement referred to above may be accidental.

Finally, the $C_1(V)$ and $L_1(V)$ RMEs interfere destructively in the cross section (see discussion at the end of Sec. II C), substantially reducing the 1S_0 channel contribution to the S -factor, see Table XVI.

B. 3S_1 Capture

The 3S_1 capture is induced by the weak axial charge and current, and weak vector current operators via the multipoles $C_1(A)$, $L_1(A)$, $E_1(A)$, and $M_1(V)$. All earlier studies only retained the dominant $L_1(A)$ and $E_1(A)$ transitions. However, as is evident from Table IX, the $M_1(V)$ and especially $C_1(A)$ RMEs are not negligible. Furthermore, the $C_1(A)$ and $L_1(A)$ RMEs interfere constructively in the cross section, since their signs are opposite. For example, neglecting the $C_1(A)$ contribution would produce an S -factor value 4.94×10^{-20} keV b, 30 % smaller than the 3S_1 total result 6.38×10^{-20} keV b (see Table XVI).

The destructive interference between the one- and many-body axial current contributions in the $L_1(A)$ and $E_1(A)$ RMEs, first obtained in Refs. [11,20], is confirmed in the present work. The axial currents associated with Δ -excitation play a crucial role. The (suppressed) one-body contribution comes mostly from transitions involving the D-state components of the ${}^3\text{He}$ and ${}^4\text{He}$ wave functions, while the many-body contributions are predominantly due to transitions connecting the S-state of ${}^3\text{He}$ to the D-state of ${}^4\text{He}$, or viceversa. To clarify this point, it is useful to define the one- and two-body densities

$$\rho^{(1)}(x) = \langle {}^4\text{He} | \sum_i \delta(x - |\mathbf{r}_i - \mathbf{R}_{jkl}|) O_i^{(1)} | p {}^3\text{He} \rangle , \quad (6.7)$$

$$\rho^{(2)}(x) = \langle {}^4\text{He} | \sum_{i<j} \delta(x - r_{ij}) O_{ij}^{(2)} | p {}^3\text{He} \rangle , \quad (6.8)$$

where $O_i^{(1)}$ is the (lowest order) Gamow-Teller operator of Eq. (4.12) at $q=0$, and $O_{ij}^{(2)}$ is the most important Δ -excitation current associated with diagrams of type (a) in Fig. 3. These densities are normalized such that

$$\int_0^\infty dx \rho^{(\alpha)}(x) = O^{(\alpha)}\text{-contribution} . \quad (6.9)$$

In Fig. 4 we display separately the contributions to $\rho^{(1)}(x)$ due to transitions involving the $L=0 \rightarrow L=0$ and $L=2 \rightarrow L=2$ components of the ${}^3\text{He}$ and ${}^4\text{He}$ wave functions. Note that the $L=0 \rightleftharpoons L=2$ transitions vanish, since the Gamow-Teller operator has no dependence on the spatial coordinates in the $q=0$ limit. The $0 \rightarrow 0$ density, while much larger than the $2 \rightarrow 2$ density, consists of positive and negative pieces, which nearly cancel out in the integral. Indeed, out of a total integral of 0.19, the $0 \rightarrow 0$ and $2 \rightarrow 2$ contributions are, respectively, 0.02 and 0.17. It is important to reemphasize that in the $0 \rightarrow 0$ integral the whole contribution comes from the mixed symmetry S' -states of the ${}^3\text{He}$ and ${}^4\text{He}$ wave functions, since the Gamow-Teller operator, in the $q=0$ limit, cannot connect their dominant (symmetric) S-states, as already pointed out in Sec. IA. This fact has been analitically verified using a simplified form for the nuclear wave functions, given by (for ${}^4\text{He}$, as an example):

$$\Psi_4 \simeq \left[1 + \sum_{i<j} u^{\sigma,4}(r_{ij}) \boldsymbol{\sigma}_i \cdot \boldsymbol{\sigma}_j + u^{t\tau,4}(r_{ij}) S_{ij} \boldsymbol{\tau}_i \cdot \boldsymbol{\tau}_j \right] \left[\prod_{i<j} f^{c,4}(r_{ij}) \right] \Phi_4 , \quad (6.10)$$

where $\Phi_4 = \det[p \uparrow_1, p \downarrow_2, n \uparrow_3, n \downarrow_4]$ is the spin-isospin Slater determinant, $f^{c,4}(r)$, $u^{\sigma,4}(r)$, and $u^{t\tau,4}(r)$ are central, spin-spin, and tensor correlation functions, respectively. The non-central terms in Eq. (6.10) generate the S' - and D-state components.

Finally, in Fig. 5, we display both the density functions $\rho^{(1)}(x)$ and $\rho^{(2)}(x)$. The density function $\rho^{(2)}(x)$, although much smaller than $\rho^{(1)}(x)$, has no zeros, and consequently its integral is comparable to that of $\rho^{(1)}(x)$.

It is interesting to examine the ‘‘small’’ M_1 RME induced by the weak vector current. It is dominated by the contributions due to two-body currents, which interfere destructively with (and, in fact, are much larger in magnitude than) those from one-body currents. This matrix element can be approximately related to that occurring in the n ${}^3\text{He}$ radiative capture at thermal neutron energies [11]. Ignoring isospin-symmetry breaking, one has

$$|p^3\text{He}\rangle \simeq \frac{C_0}{\sqrt{2}} T_+ |T=1, M_T=0\rangle, \quad (6.11)$$

and hence, in a schematic notation,

$$\begin{aligned} \langle {}^4\text{He} | \hat{\mathbf{e}}_\lambda^* \cdot \mathbf{j}_z^\dagger(\gamma) | n^3\text{He}\rangle &\simeq \frac{1}{\sqrt{2}} \langle {}^4\text{He} | \hat{\mathbf{e}}_\lambda^* \cdot \mathbf{j}_z^\dagger(\gamma) | T=1, M_T=0\rangle \\ &\simeq -\frac{1}{2C_0} \langle {}^4\text{He} | \hat{\mathbf{e}}_\lambda^* \cdot \mathbf{j}_+^\dagger(V) | p^3\text{He}\rangle \end{aligned} \quad (6.12)$$

where C_0 is the Gamow penetration factor, $\mathbf{j}_z(\gamma)$ is the electromagnetic current, and use has been made of the CVC relation to relate the commutator $[T_+, \mathbf{j}_+^\dagger(V)]$ to $\mathbf{j}_z^\dagger(\gamma)$. Note that in the first line of Eq. (6.12) the contribution from the $T, M_T = 0, 0$ (1+3)-state has been neglected, since the isoscalar magnetic moment of the nucleon is a factor $\simeq 5$ smaller than the isovector one, and the dominant two-body electromagnetic currents are isovector. On the basis of Eq. (6.12), one would predict $n^3\text{He}$ radiative capture cross sections, at zero energy, of $227 \mu\text{b}$, $142 \mu\text{b}$, and $480 \mu\text{b}$ with one-body, one- plus two-body, and full currents—the latter include the Δ -excitation currents treated in perturbation theory (PT), which severely overestimates their contribution [11]. The value $480 \mu\text{b}$ is almost an order of magnitude larger than the measured cross section, $(55 \pm 3)\mu\text{b}$ [16]. Ignoring the Δ contribution, for which the PT estimate is known to be unrealistic, the result obtained with one- and two-body currents (the model-independent ones of Sec. IV A), $142 \mu\text{b}$, is still too large by a factor $\simeq 2.6$. However, the approximations made in Eqs. (6.11)–(6.12) are presumably too rough for a reaction as delicate as the $n^3\text{He}$ capture (see discussion in Sec. I A). Indeed, this process provides a sensitive testing ground for models of interactions and currents. A calculation of its cross section with CHH wave functions is currently underway.

In Table X we list the one-body axial current contributions at two values of q , 0 and 19.2 MeV/c, corresponding to the lowest and highest momentum transfers allowed by the $p^3\text{He}$ kinematics. A number of comments are in order. Firstly, the RME associated with the Gamow-Teller operator, labelled NR in the table, has a rather strong dependence on q . At $q=0$ this RME is suppressed (see discussion above). When $q > 0$, however, the next term in the expansion of the plane wave in Eq. (4.12) leads to an operator having the structure $\tau_{i,\pm} \boldsymbol{\sigma}_i r_{i,z}^2$, which can connect the “large” S- and D-state components of the bound-state wave functions. Its contribution, although of order $(qR)^2 \simeq 0.02$ ($R \simeq 1.4$ fm is the α -particle radius), is not negligible. Secondly, the suppression mechanism referred to above also makes the relativistic corrections to the Gamow-Teller operator of Eq. (4.13) relatively important. Thirdly, the induced pseudoscalar term, last term in Eq. (4.13), is purely longitudinal, and itself suppressed, since it is proportional to the NR operator.

In Table XI we report the cumulative contributions to the $L_1(\text{A})$ and $E_1(\text{A})$ RMEs at $q=0$ and 19.2 MeV/c. The momentum transfer dependence of the results originates from that of the one-body currents, the mesonic and Δ -excitation current contributions are, in fact, very weakly dependent on q . Note that the results obtained by treating the Δ -currents either with the TCO method or in perturbation theory (PT) differ by 1–2 %. This is because the $N\Delta$ axial coupling constant g_A^* is determined by fitting, independently in the TCO and PT schemes, the Gamow-Teller matrix element of tritium β -decay. This procedure severely reduces the model dependence of the weak axial current. Finally, we note that, if

the quark model value were to be used for g_A^* ($g_A^* = 6\sqrt{2}/5g_A$), the $L_1(A)$ ($E_1(A)$) RME at $q=19.2$ MeV/c would have been -0.489×10^{-1} (-0.716×10^{-1}) using the TCO method and -0.150×10^{-1} (-0.234×10^{-1}) in the PT treatment, respectively.

C. P-wave Capture

There are four P-wave capture channels: 3P_0 , 1P_1 , 3P_1 , and 3P_2 . Note that 1P_1 and 3P_1 are coupled channels (see Sec. III C). The 3P_0 capture is induced by the weak axial charge and the longitudinal component of the weak axial current via the $C_0(A)$ and $L_0(A)$ multipoles, respectively. The associated RMEs, as defined in Eq. (6.1), are listed in Table XII. The two-body axial charge operators of Sec. IV D, among which the pion-exchange term is dominant, give a $\simeq 20$ % correction to the one-body contribution in the $C_0(A)$ RME. The $L_0(A)$ RME is about 40 % of, and has the same sign as, the $C_0(A)$ RME. This positive relative sign produces a destructive interference between these RMEs in the cross section, substantially reducing the 3P_0 overall contribution to the S -factor, as discussed in Sec. II C. The $C_0(A)$ and $L_0(A)$ RMEs are expected to have the same sign, as justified by the following argument. The $C_0(q; A)$ multipole operator can be written, in the $q \rightarrow 0$ limit, as

$$\begin{aligned} C_0(q; A) &\rightarrow -\frac{1}{\sqrt{4\pi}} \frac{g_A}{2m} \sum_i \left[\tau_{i,\pm} \boldsymbol{\sigma}_i \cdot \mathbf{p}_i \right]_+ \\ &\simeq \frac{i}{\sqrt{4\pi}} \frac{g_A}{2} \sum_i \left[\tau_{i,\pm} \boldsymbol{\sigma}_i \cdot \mathbf{r}_i, H \right], \end{aligned} \quad (6.13)$$

where we have used the approximate relation $\mathbf{p}_i \simeq -im[\mathbf{r}_i, H]$ (violated by the momentum-dependent components of the two-nucleon interaction), and in the second line of Eq. (6.13) have ignored, in a rather cavalier fashion, terms like $\tau_{i,\pm} \boldsymbol{\sigma}_i \cdot H\mathbf{r}_i - \mathbf{r}_i H \cdot \boldsymbol{\sigma}_i \tau_{i,\pm}$. For the $L_0(q; A)$ multipole we find in the same limit

$$L_0(q; A) \rightarrow \frac{i}{\sqrt{4\pi}} \frac{g_A}{3} q \sum_i \tau_{i,\pm} \boldsymbol{\sigma}_i \cdot \mathbf{r}_i, \quad (6.14)$$

and therefore we would expect the $C_0(A)$ and $L_0(A)$ RMEs to be approximately in the ratio

$$\frac{C_0(A)}{L_0(A)} \simeq \frac{3E_3 - E_4}{2q}, \quad (6.15)$$

which, given the rather severe approximations made in deriving Eq. (6.13), is reasonably close to the (one-body) value obtained in the calculation (1.6 versus 2.0).

The 1P_1 and 3P_1 captures are induced by the weak vector charge and current, and weak axial current via the multipoles $C_1(V)$, $L_1(V)$, $E_1(V)$, and $M_1(A)$. The calculated values for the associated RMEs are listed in Tables XIII and XIV. The RME magnitudes of the weak vector transitions in 3P_1 capture are much smaller than those in 1P_1 capture. In the long-wavelength approximation, the one-body $C_1(V)$, $L_1(V)$, and $E_1(V)$ multipoles are independent of spin, and therefore cannot connect the dominant part of the 3P_1 wave function, which has total spin $S=1$, to the S-wave component of ${}^4\text{He}$, which has $S=0$. This is not the case for the 1P_1 channel, in which the total spin $S=0$ term is in fact largest. Indeed,

because of this suppression, the two-body weak vector charge and current contributions are found to be dominant in ${}^3\text{P}_1$ capture. The situation is reversed for the axial transition, since there the spin-flip nature of the $M_1(A)$ multipole makes the associated RME in ${}^3\text{P}_1$ larger than that in ${}^1\text{P}_1$ (in absolute value).

The $E_1(V)$ operator can be shown to have the long-wavelength form [18]

$$E_1(q; V) = -\frac{\sqrt{2}}{q} [H, C_1(q; V)] , \quad (6.16)$$

and so the $E_1(V)$ and $C_1(V)$ RMEs would be expected to be in the ratio

$$\frac{E_1(q; V)}{C_1(q; V)} \simeq \sqrt{2} \frac{E_3 - E_4}{q} \simeq 1.51 , \quad (6.17)$$

assuming the validity of the long-wavelength approximation, and that the CHH wave functions are truly exact eigenfunctions of the Hamiltonian. We reiterate here that the currents used in the present work satisfy the continuity equation only with the v_6 part of the AV14 and AV18 interactions, namely in momentum space $\mathbf{q} \cdot \mathbf{j}(\mathbf{q}; V) = [T + v_6, \rho_{\text{NR}}^{(1)}(\mathbf{q}; V)]$. The currents induced by the momentum dependent components of the interactions, such as the spin-orbit term, have been neglected. Thus the ratio obtained in the calculation is 1.34 for the ${}^1\text{P}_1$ channel, somewhat smaller than the expected value presumably because of the “missing” currents and the approximate eigenstate property satisfied by the present CHH (variational) wave functions. These same cautionary remarks also apply to the comparison between the $C_1(V)$ and $L_1(V)$ RMEs, which should be related to each other via Eq. (6.6).

The situation is more delicate in ${}^3\text{P}_1$ capture, since this transition is suppressed. Here the long-wavelength approximation of the $E_1(V)$ multipole is inadequate, and higher order terms in the power expansion in q need to be retained, so called retardation terms. In fact the situation is closely related to that of electric dipole transitions in pd radiative capture at very low energies (0–100 keV). We refer the reader to Ref. [18] for a thorough discussion of these issues.

The ${}^3\text{P}_2$ capture is induced by the weak axial charge and current, and weak vector current operators via the multipoles $C_2(A)$, $L_2(A)$, $E_2(A)$, and $M_2(V)$. The associated RMEs are listed in Table XV. The $L_2(A)$ and $E_2(A)$ RMEs are comparable to the $L_1(A)$ and $E_1(A)$ RMEs in ${}^3\text{S}_1$ capture, and are dominated by the contributions of one-body currents. In fact, the latter can now connect the large S-wave components of the three- and four-nucleon bound states. The density function $\rho^{(1)}(x)$, defined in analogy to Eq. (6.7) (but for the ${}^3\text{P}_2$ channel), is displayed in Fig. 6, and should be compared to that in Fig. 5 for ${}^3\text{S}_1$ capture. While smaller in magnitude than the latter—after all, the ${}^3\text{P}_2$ transition is inhibited with respect to the ${}^3\text{S}_1$ transition by a factor $\simeq qR$ and the presence of the centrifugal barrier—the ${}^3\text{P}_2$ density has the same sign, and therefore its integral turns out to be comparable to that of the ${}^3\text{S}_1$ density.

D. Model Dependence

In Table XVI we list, for all S- and P-wave channels, the S -factor values obtained with the AV18/UIX, AV18, and AV14/UVIII interactions. Note that the sum of the channel

contributions is a few % smaller than the total result reported at the bottom of the table (see end of Sec. II C). The $N\Delta$ axial coupling constant is determined by fitting the Gamow-Teller matrix element in tritium β -decay, within each given Hamiltonian model. As a result of this procedure the model dependence of the S -factor predictions is substantially reduced.

Inspection of Table XVI shows that inclusion of the three-nucleon interaction reduces the total S -factor by about 20 % (compare the AV18 and AV18/UIX results). This decrease is mostly in the 3S_1 contribution, and can be traced back to a corresponding reduction in the magnitude of the one-body axial current matrix elements. The latter are sensitive to the triplet scattering length, for which the AV18 and AV18/UIX models predict, respectively, 10.0 fm and 9.13 fm (see Table III).

The comparison between the AV18/UIX and AV14/UVIII models, which both reproduce the measured bound-state properties and low-energy scattering parameters of the three- and four-nucleon systems, suggests a rather weak model dependence. It is important to reiterate that this is accomplished by virtue of the procedure used to constrain the axial current. Indeed, the AV18/UIX and AV14/UVIII 3S_1 contributions to the S -factor obtained with one-body currents only are, respectively, 26.4×10^{-20} keV b and 35.8×10^{-20} keV b. This difference is presumably due to the stronger tensor component of AV14 as compared to that of AV18.

Finally, the 3S_1 contribution to the S -factor obtained with the AV14/UVIII model in the present work, 6.60×10^{-20} keV b, is to be compared with the older prediction of Ref. [11], 1.3×10^{-20} keV b. It is important to point out that the older calculation (i) used the long-wavelength form of the $E_1(A)$ and $L_1(A)$ operators, (ii) ignored the contributions of transitions induced by the axial charge and vector current, (iii) retained only the leading non-relativistic (Gamow-Teller) term of the single-nucleon axial current, and (iv) employed bound and continuum wave functions, obtained with the Variational Monte Carlo (VMC) method. In regard to this last point, we note that, for example, the $\overline{E}_1(q=0; A)$ RME calculated in Ref. [11] with the Gamow-Teller operator is 0.613×10^{-1} fm $^{3/2}$ versus a value of 0.119 fm $^{3/2}$ obtained here. The factor $\simeq 2$ increase is only due to differences in the wave functions. The present CHH wave functions are expected to be more accurate than the VMC wave functions of Ref. [11].

ACKNOWLEDGMENTS

The authors wish to thank V.R. Pandharipande, D.O. Riska, P. Vogel, and R.B. Wiringa for useful discussions, and J. Carlson for a critical reading of the manuscript. M.V. and R.S. acknowledge partial financial support of NATO through the Collaborative Research Grant No. 930741. The support of the U.S. Department of Energy under contract number DE-AC05-84ER40150 is gratefully acknowledged by L.E.M. and R.S. Finally, some of the calculations were made possible by grants of computing time from the National Energy Research Supercomputer Center in Livermore.

REFERENCES

- [1] J.N. Bahcall and P.I. Krastev, Phys. Lett. B **436**, 243 (1998).
- [2] G. Fiorentini, V. Berezinsky, S. Degl'Innocenti, and B. Ricci, Phys. Lett. B **444**, 387 (1998).
- [3] R. Escribano, J.M. Frère, A. Gevaert, and P. Monderen, Phys. Lett. B **444**, 397 (1998).
- [4] C.J. Horowitz, Phys. Rev. C **60**, 022801 (1999).
- [5] W.M. Alberico, S.M. Bilenky, and W. Grimus, hep-ph/0001245.
- [6] W.M. Alberico, J. Barnabéu, S.M. Bilenky, and W. Grimus, Phys. Lett. B **478**, 208 (2000).
- [7] Y. Fukuda *et al.*, Phys. Rev. Lett. **82**, 2430 (1999).
- [8] M.B. Smy, hep-ex/9903034.
- [9] Y. Suzuki, contribution to Lepton-Photon Symposium 99 (1999), <http://www-sk.icrr.u-tokyo.ac.jp/doc/sk/pub/index.html>.
- [10] J.N. Bahcall, S. Basu, and M.H. Pinsonneault, Phys. Lett. B **433**, 1 (1998).
- [11] R. Schiavilla, R.B. Wiringa, V.R. Pandharipande, and J. Carlson, Phys. Rev. C **45**, 2628 (1992).
- [12] S.P. Mikheev and A.Y. Smirnov, Nuovo Cim. **9C**, 17 (1986).
- [13] A.E. Cox, S.A.R. Wynchank, and C.H. Collie, Nucl. Phys. **74**, 497 (1965).
- [14] E.T. Jurney, P.J. Bendt, and J.C. Browne, Phys. Rev. C **25**, 2810 (1982).
- [15] F.L.H. Wolfs, S.J. Freedman, J.E. Nelson, M.S. Dewey, and G.L. Greene, Phys. Rev. Lett. **63**, 2721 (1989).
- [16] R. Wervelman, K. Abrahams, H. Postma, J.G.L. Booten, and A.G.M. Van Hees, Nucl. Phys. **A526**, 265 (1991).
- [17] L.I. Schiff, Phys. Rev. **52**, 242 (1937).
- [18] M. Viviani, A. Kievsky, L.E. Marcucci, S. Rosati, and R. Schiavilla, Phys. Rev. C **61**, 064001 (2000).
- [19] J. Carlson, D.O. Riska, R. Schiavilla, and R.B. Wiringa, Phys. Rev. C **42**, 830 (1990).
- [20] J. Carlson, D.O. Riska, R. Schiavilla, and R.B. Wiringa, Phys. Rev. C **44**, 619 (1991).
- [21] M. Chemtob and M. Rho, Nucl. Phys. **A163**, 1 (1971).
- [22] I.S. Towner, Phys. Rep. **155**, 263 (1987).
- [23] C. Werntz and J.G. Brennan, Phys. Rev. C **8**, 1545 (1973).
- [24] E.E. Salpeter, Phys. Rev. **88**, 547 (1952).
- [25] V.A. Kuzmin, Phys. Lett. **17**, 27 (1965).
- [26] C. Werntz and J.G. Brennan, Phys. Rev. **157**, 759 (1967).
- [27] P.E. Tegnér and C. Bargholtz, Astrophys. J. **272**, 311 (1983).
- [28] R.B. Wiringa, V.G.J. Stoks, and R. Schiavilla, Phys. Rev. C **51**, 38 (1995).
- [29] B.S. Pudliner, V.R. Pandharipande, J. Carlson, and R.B. Wiringa, Phys. Rev. Lett. **74**, 4396 (1995).
- [30] R.B. Wiringa, R.A. Smith, and T.L. Ainsworth, Phys. Rev. C **29**, 1207 (1984).
- [31] R.B. Wiringa, Phys. Rev. C **43**, 1585 (1991).
- [32] B.S. Pudliner, V.R. Pandharipande, J. Carlson, S.C. Pieper, and R.B. Wiringa, Phys. Rev. C **56**, 1720 (1997).
- [33] J. Carlson, private communication.
- [34] M. Viviani, A. Kievsky, and S. Rosati, Few-Body Syst. **18**, 25 (1995).
- [35] M. Viviani, S. Rosati, and A. Kievsky, Phys. Rev. Lett. **81**, 1580 (1998).

- [36] M. Viviani, private communication.
- [37] A. Kievsky *et al.*, Phys. Rev. C **58**, 3085 (1998).
- [38] W. Glöckle *et al.*, Phys. Rep. **274**, 107 (1996), and references therein; A. Kievsky, Phys. Rev. C **60**, 034001 (1999).
- [39] M. Viviani, Nucl. Phys. **A631**, 111c (1998).
- [40] T.W. Phillips, B.L. Berman, and J.D. Seagrave, Phys. Rev. C **22**, 384 (1980).
- [41] M.T. Alley and L.D. Knutson, Phys. Rev. C **48**, 1901 (1993).
- [42] L.E. Marcucci, D.O. Riska, and R. Schiavilla, Phys. Rev. C **58**, 3069 (1998).
- [43] K. Kubodera, J. Delorme, and M. Rho, Phys. Rev. Lett. **40**, 755 (1978).
- [44] M. Kirchbach, D.O. Riska, and K. Tsushima, Nucl. Phys. **A542**, 616 (1992).
- [45] R. Schiavilla *et al.*, Phys. Rev. C **58**, 1263 (1998).
- [46] R. Machleidt, F. Sammarruca, and Y. Song, Phys. Rev. C **53**, 1483 (1996).
- [47] J. N. Bahcall, E. Lisi, D.E. Alburger, L. De Braekeleer, S.J. Freedman, and J. Napolitano, Phys. Rev. C **54**, 411 (1996).
- [48] <http://www.sns.ias.edu/~jnb>.
- [49] M. Nakahata *et al.*, Nucl. Instrum. Methods Phys. Res., Sect. A **421**, 113 (1999).
- [50] J.F. Beacom and P. Vogel, Phys. Rev. Lett. **83**, 5222 (1999).
- [51] C.E. Ortiz *et al.*, nucl-ex/0003006.
- [52] J.D. Walecka, *Theoretical Nuclear and Subnuclear Physics* (Oxford University Press, New York, 1995).
- [53] J.C. Hardy, I.S. Towner, V.T. Koslowsky, E. Hagberg, and H. Schmeing, Nucl. Phys. **A509**, 429 (1990).
- [54] J.D. Bjorken and S.D. Drell, *Relativistic Quantum Mechanics* (McGraw-Hill, New York, 1964).
- [55] A.R. Edmonds, *Angular Momentum in Quantum Mechanics* (Princeton University Press, Princeton, 1957).
- [56] A. Kievsky, M. Viviani, and S. Rosati, Nucl. Phys. **A551**, 241 (1993).
- [57] A. Kievsky, M. Viviani, and S. Rosati, Nucl. Phys. **A577**, 511 (1994).
- [58] A. Kievsky, M. Viviani, and S. Rosati, Phys. Rev. C **52**, R15 (1995).
- [59] H.J. Karwowski, private communication.
- [60] E. George and L.D. Knutson, private communication.
- [61] D.R. Tilley, H.R. Weller, and G.M. Hale, Nucl. Phys. **A541**, 1 (1992).
- [62] K.F. Famularo *et al.*, Phys. Rev. **93**, 928 (1954).
- [63] M. Viviani, A. Kievsky, and S. Rosati, in preparation.
- [64] T. deForest and J.D. Walecka, Adv. Phys. **15**, 1 (1966).
- [65] J.L. Friar, Ann. Phys. (N.Y.) **81**, 332 (1973).
- [66] E. Adelberger *et al.*, Rev. Mod. Phys. **70**, 1265 (1998).
- [67] Particle Data Group, R.M. Barnett *et al.*, Phys. Rev. D **54**, 1 (1996).
- [68] H. Abele *et al.*, Phys. Lett. B **407**, 212 (1997).
- [69] M. Gmitro and P. Truöl, Adv. Nucl. Phys. **18**, 241 (1987).
- [70] R. Schiavilla, D.O. Riska, and V.R. Pandharipande, Phys. Rev. C **40**, 2294 (1989).
- [71] R. Schiavilla, D.O. Riska, and V.R. Pandharipande, Phys. Rev. C **41**, 309 (1990).
- [72] D.O. Riska, Phys. Rep. **181**, 207 (1989).
- [73] R. Schiavilla and D.O. Riska, Phys. Rev. C **43**, 437 (1991).
- [74] R.B. Wiringa and R. Schiavilla, Phys. Rev. Lett. **81**, 4317 (1998).

- [75] M. Viviani, R. Schiavilla, and A. Kievsky, *Phys. Rev. C* **54**, 534 (1996).
- [76] M. Garçon, private communication; D. Abbott *et al.*, nucl-ex/0001006 and nucl-ex/0002003.
- [77] J. Carlson and R. Schiavilla, *Rev. Mod. Phys.* **70**, 743 (1998).
- [78] J.L. Friar, *Ann. Phys. (N.Y.)* **104**, 380 (1977).
- [79] R. Schiavilla, *Perspectives in Nuclear Physics at Intermediate Energies*, edited by S. Boffi, C. Ciofi degli Atti, and M. Giannini (World Scientific, Singapore, 1996), p. 490.
- [80] R. Schiavilla and R.B. Wiringa, to be published.
- [81] R. Machleidt, *Adv. Nucl. Phys.* **19**, 189 (1989).
- [82] E.K. Warburton, *Phys. Rev. Lett.* **66**, 1823 (1991); *Phys. Rev. C* **44**, 233 (1991).
- [83] I.S. Towner, *Nucl. Phys.* **A542**, 631 (1992).
- [84] R.B. Wiringa, private communication.
- [85] V.G.J. Stoks, R.A.M. Klomp, M.C.M. Rentmeester, and J.J. de Swart, *Phys. Rev. C* **48**, 792 (1993).
- [86] In Ref. [45] the relativistic corrections to the single-nucleon axial current operator in Eq. (4.13) were neglected. Furthermore, in the calculation of the contribution of the ρ -exchange axial current operator, the non-local term (proportional to \mathbf{P}_i) in the second line of Eq. (4.33) was inadvertently omitted. However, this has no impact on the conclusions of that work, since the non-local term referred to above was also omitted in the calculation of the pp capture cross section.
- [87] C.E. Carlson, *Phys. Rev. D* **34**, 2704 (1986).
- [88] D. Lin and M.K. Liou, *Phys. Rev. C* **43**, R930 (1991).
- [89] N. Metropolis, A.W. Rosenbluth, M.N. Rosenbluth, A.H. Teller, and E. Teller, *J. Chem. Phys.* **21**, 1087 (1953).

TABLES

TABLE I. The *hep* *S*-factor, in units of 10^{-20} keV b, calculated with CHH wave functions corresponding to the AV18/UIX Hamiltonian model, at $p^3\text{He}$ c.m. energies $E=0, 5,$ and 10 keV. The rows labelled “one-body” and “full” list the contributions obtained by retaining the one-body only and both one- and many-body terms in the nuclear weak current. The contributions due the $^3\text{S}_1$ channel only and all S- and P-wave channels are listed separately.

	$E=0$ keV		$E=5$ keV		$E=10$ keV	
	$^3\text{S}_1$	S+P	$^3\text{S}_1$	S+P	$^3\text{S}_1$	S+P
one-body	26.4	29.0	25.9	28.7	26.2	29.3
full	6.38	9.64	6.20	9.70	6.36	10.1

TABLE II. Binding energies in MeV of ^4He calculated with the CHH method using the AV18 and AV18/UIX, and the older AV14 and AV14/UVIII, Hamiltonian models. Also listed are the corresponding “exact” GFMC results [32,33] and the experimental value.

Model	CHH	GFMC
AV18	24.01	24.1(1)
AV18/UIX	27.89	28.3(1)
AV14	23.98	24.2(2)
AV14/UVIII	27.50	28.3(2)
EXP		28.3

TABLE III. Binding energies, B_3 , of ^3He , and $p^3\text{He}$ singlet and triplet S-wave scattering lengths, a_s and a_t , calculated with the CHH method using the AV18 and AV18/UIX, and the older AV14 and AV14/UVIII, Hamiltonian models. The corresponding experimental values are also listed.

Model	$B_3(\text{MeV})$	$a_s(\text{fm})$	$a_t(\text{fm})$
AV14	7.03		
AV18	6.93	12.9	10.0
AV14/UVIII	7.73		9.24
AV18/UIX	7.74	11.5	9.13
EXP	7.72	10.8 ± 2.6 [41]	8.1 ± 0.5 [41] 10.2 ± 1.5 [27]

TABLE IV. Phase-shift and mixing-angle parameters (in deg) for $p^3\text{He}$ elastic scattering at c.m. energy of 1.2 MeV, calculated with the CHH method using the AV18 and AV18/UIX Hamiltonian models. The corresponding experimental values obtained in the phase-shift analysis of Ref. [41] are also listed.

parameter	AV18	AV18/UIX	PSA
$^1\text{S}_0$	-33.3	-31.3	-27.4 ± 3.5
$^3\text{S}_1$	-28.8	-27.1	-26.5 ± 0.6
$^3\text{P}_0$	4.1	3.2	2.6 ± 0.6
$^3\text{P}_1$	8.1	7.4	10.1 ± 0.5
$^3\text{P}_2$	7.7	6.9	8.9 ± 0.5
$^1\text{P}_1$	6.5	5.5	4.2 ± 1.5
$\epsilon(1^-)$	-14.7	-13.2	-7.8 ± 0.6

TABLE V. Contributions to the Gamow-Teller (GT) matrix element of tritium β -decay, obtained with the CHH trinucleon wave functions corresponding to the AV18/UIX Hamiltonian model. The rows labelled “one-body NR” and “one-body RC” list the contributions associated with the single-nucleon axial current operators of Eq. (4.12) and Eq. (4.13), respectively, while the row labelled “mesonic” lists the sum of the contributions due to the π -, ρ -, and $\rho\pi$ -exchange axial current operators of Eqs. (4.32)–(4.34) with cutoff masses $\Lambda_\pi = 4.8 \text{ fm}^{-1}$ and $\Lambda_\rho = 6.8 \text{ fm}^{-1}$. Finally, the rows labelled “ Δ - g_A^* ”, “ Δ - \bar{g}_A ”, and “ Δ -renormalization” list, respectively, the contributions associated with panels (a)-(b), (c)-(d) and (f), and (e) and (g)-(j), of Fig. 3. The cumulative result reproduces the “experimental value” 0.957 for the GT matrix element [45], once the change in normalization of the wave functions due to the presence of Δ -components is taken into account.

	GT matrix element
one-body NR	0.9218
one-body RC	-0.0084
mesonic	0.0050
Δ - g_A^*	0.0509
Δ - \bar{g}_A	0.0028
Δ -renormalization	0.0074

TABLE VI. The values of the $N \rightarrow \Delta$ axial coupling constant g_A^* in units of g_A , when the Δ -isobar degrees of freedom are treated in perturbation theory (PT), or in the context of a TCO calculation based on the AV28Q interaction. The purely nucleonic CHH wave functions correspond to the AV18/UIX Hamiltonian model.

Δ -isobar treatment	g_A^*/g_A
PT	1.224
TCO	2.868

TABLE VII. The wave function normalization ratios $\langle \Psi_{N+\Delta} | \Psi_{N+\Delta} \rangle / \langle \Psi | \Psi \rangle$ obtained for the bound three- and four-nucleon systems, when the TCO calculation is based on the AV28Q interaction. The purely nucleonic CHH wave functions $|\Psi\rangle$ correspond to the AV18/UIX Hamiltonian model.

Model	${}^3\text{H}$	${}^3\text{He}$	${}^4\text{He}$
AV28Q	1.0238	1.0234	1.0650

TABLE VIII. Cumulative contributions to the reduced matrix elements (RMEs) $\overline{C}_0(q; V)$ and $\overline{L}_0(q; V)$ in ${}^1\text{S}_0$ capture at zero p ${}^3\text{He}$ c.m. energy. The momentum transfer q is 19.2 MeV/c, and the results correspond to the AV18/UIX Hamiltonian model. The row labelled “one-body” lists the contributions associated with the operators in Eq. (4.5) for the weak vector charge $\rho(V)$ and Eq. (4.8) for the weak vector current $\mathbf{j}(V)$; the row labelled “mesonic” lists the results obtained by including, in addition, the contributions associated with the operators in Eqs. (4.30)–(4.31) for $\rho(V)$, and Eqs. (4.16)–(4.17) for $\mathbf{j}(V)$. The Δ terms in $\rho(V)$ are neglected, while those in $\mathbf{j}(V)$ are purely transverse and therefore do not contribute to the \overline{L}_0 RME. Note that the RMEs are purely real and in $\text{fm}^{3/2}$ units.

	$\overline{C}_0(q; V)$	$\overline{L}_0(q; V)$
one-body	-0.857×10^{-2}	-0.864×10^{-2}
mesonic	-0.856×10^{-2}	-0.919×10^{-2}

TABLE IX. Cumulative contributions to the reduced matrix elements (RMEs) $\overline{C}_1(q; A)$, $\overline{L}_1(q; A)$, $\overline{E}_1(q; A)$ and $\overline{M}_1(q; V)$ in ${}^3\text{S}_1$ capture at zero p ${}^3\text{He}$ c.m. energy. The momentum transfer q is 19.2 MeV/c, and the results correspond to the AV18/UIX Hamiltonian model. The row labelled “one-body” lists the contributions associated with the operators in Eq. (4.10) for the weak axial charge $\rho(A)$, Eq. (4.11) for the weak axial current $\mathbf{j}(A)$, and Eq. (4.8) for the weak vector current $\mathbf{j}(V)$; the row labelled “mesonic” lists the results obtained by including, in addition, the contributions associated with the operators in Eqs. (4.35)–(4.37) for $\rho(A)$, Eqs. (4.32)–(4.34) for $\mathbf{j}(A)$, and Eqs. (4.16)–(4.17) for $\mathbf{j}(V)$; finally, the row labelled “ Δ ” lists the results obtained by also including the contributions of the operators in Eqs. (4.50)–(4.51) for $\rho(A)$, Eqs. (4.48)–(4.49) for $\mathbf{j}(A)$, and Eqs. (4.52)–(4.53) for $\mathbf{j}(V)$. The Δ contributions in both $\rho(A)$ and $\mathbf{j}(A)$ are calculated with the TCO method, and take into account the change in normalization of the wave functions due to the presence of Δ -components. Those in $\mathbf{j}(V)$ are calculated in perturbation theory. Note that the RMEs are purely imaginary and in $\text{fm}^{3/2}$ units.

	$\overline{C}_1(q; A)$	$\overline{L}_1(q; A)$	$\overline{E}_1(q; A)$	$\overline{M}_1(q; V)$
one-body	0.147×10^{-1}	-0.730×10^{-1}	-0.106	0.333×10^{-2}
mesonic	0.156×10^{-1}	-0.679×10^{-1}	-0.984×10^{-1}	-0.263×10^{-2}
Δ	0.155×10^{-1}	-0.293×10^{-1}	-0.440×10^{-1}	-0.484×10^{-2}

TABLE X. One-body contributions, at momentum transfers $q=0$ and 19.2 MeV/c, to the reduced matrix elements (RMEs) $\overline{L}_1(q; A)$ and $\overline{E}_1(q; A)$ in 3S_1 capture at zero p ${}^3\text{He}$ c.m. energy. The results correspond to the AV18/UIX Hamiltonian model. The rows labelled “NR” and “RC” list the contributions obtained with the operators of Eq. (4.12) and Eq. (4.13), respectively; the row labelled “IPS” lists the contribution of the induced pseudoscalar current only (last term in Eq. (4.13)). Note that the RMEs are purely imaginary and in $\text{fm}^{3/2}$ units.

	$\overline{L}_1(q; A)$		$\overline{E}_1(q; A)$	
	$q=0$ MeV/c	$q=19.2$ MeV/c	$q=0$ MeV/c	$q=19.2$ MeV/c
NR	-0.726×10^{-1}	-0.586×10^{-1}	-0.103	-0.838×10^{-1}
RC	-0.154×10^{-1}	-0.145×10^{-1}	-0.220×10^{-1}	-0.219×10^{-1}
IPS		0.741×10^{-3}		

TABLE XI. Cumulative contributions, at momentum transfers $q=0$ and 19.2 MeV/c, to the reduced matrix elements (RMEs) $\overline{L}_1(q; A)$ and $\overline{E}_1(q; A)$ of the weak axial current in 3S_1 capture at zero p ${}^3\text{He}$ c.m. energy. The results correspond to the AV18/UIX Hamiltonian model. The row labelled “one-body” lists the contributions associated with the operator in Eq. (4.11); the row labelled “mesonic” lists the results obtained by including, in addition, the contributions associated with the operators in Eqs. (4.32)–(4.34); finally, the rows labelled “ Δ -TCO” and Δ -PT list the results obtained by also including the contributions of the operators in Eqs. (4.48)–(4.49), calculated either in the TCO scheme or in perturbation theory (PT). The Δ -TCO results also take into account the change in normalization of the wave functions due to the presence of Δ -components. Note that the RMEs are purely imaginary and in $\text{fm}^{3/2}$ units.

	$\overline{L}_1(q; A)$		$\overline{E}_1(q; A)$	
	$q=0$ MeV/c	$q=19.2$ MeV/c	$q=0$ MeV/c	$q=19.2$ MeV/c
one-body	-0.880×10^{-1}	-0.730×10^{-1}	-0.125	-0.106
mesonic	-0.829×10^{-1}	-0.679×10^{-1}	-0.117	-0.984×10^{-1}
Δ -TCO	-0.440×10^{-1}	-0.293×10^{-1}	-0.625×10^{-1}	-0.440×10^{-1}
Δ -PT	-0.447×10^{-1}	-0.298×10^{-1}	-0.631×10^{-1}	-0.443×10^{-1}

TABLE XII. Cumulative contributions to the reduced matrix elements (RMEs) $\overline{C}_0(q; A)$ and $\overline{L}_0(q; A)$ in ${}^3\text{P}_0$ capture at zero $p^3\text{He}$ c.m. energy. The momentum transfer q is 19.2 MeV/c, and the results correspond to the AV18/UIX Hamiltonian model. The row labelled “one-body” lists the contributions associated with the operators in Eq. (4.10) for the weak axial charge $\rho(A)$ and Eq. (4.11) for the weak axial current $\mathbf{j}(A)$; the row labelled “mesonic” lists the results obtained by including, in addition, the contributions associated with the operators in Eqs. (4.35)–(4.37) for $\rho(A)$, and Eqs. (4.32)–(4.34) for $\mathbf{j}(A)$; finally, the row labelled “ Δ ” lists the results obtained by also including the contributions of the operators in Eqs. (4.50)–(4.51) for $\rho(A)$, and Eqs. (4.48)–(4.49) for $\mathbf{j}(A)$. The Δ contributions in both $\rho(A)$ and $\mathbf{j}(A)$ are calculated with the TCO method, and take into account the change in normalization of the wave functions due to the presence of Δ -components. Note that the RMEs are purely imaginary and in $\text{fm}^{3/2}$ units.

	$\overline{C}_0(q; A)$	$\overline{L}_0(q; A)$
one-body	0.371×10^{-1}	0.182×10^{-1}
mesonic	0.444×10^{-1}	0.183×10^{-1}
Δ	0.459×10^{-1}	0.188×10^{-1}

TABLE XIII. Cumulative contributions to the reduced matrix elements (RMEs) $\overline{C}_1(q; V)$, $\overline{L}_1(q; V)$, $\overline{E}_1(q; V)$ and $\overline{M}_1(q; A)$ in ${}^1\text{P}_1$ capture at zero $p^3\text{He}$ c.m. energy. The momentum transfer q is 19.2 MeV/c, and the results correspond to the AV18/UIX Hamiltonian model. The row labelled “one-body” lists the contributions associated with the operators in Eq. (4.5) for the weak vector charge $\rho(V)$, Eq. (4.8) for the weak vector current $\mathbf{j}(V)$, and Eq. (4.11) for the weak axial current $\mathbf{j}(A)$; the row labelled “mesonic” lists the results obtained by including, in addition, the contributions associated with the operators in Eqs. (4.30)–(4.31) for $\rho(V)$, Eqs. (4.16)–(4.17) for $\mathbf{j}(V)$, and Eqs. (4.32)–(4.34) for $\mathbf{j}(A)$; finally, the row labelled “ Δ ” lists the results obtained by also including the contributions of the operators in Eqs. (4.52)–(4.53) for $\mathbf{j}(V)$, and Eqs. (4.48)–(4.49) for $\mathbf{j}(A)$. The Δ contributions in $\mathbf{j}(A)$ are calculated with the TCO method, and take into account the change in normalization of the wave functions due to the presence of Δ -components. Those in $\mathbf{j}(V)$ are calculated in perturbation theory. The Δ terms in $\rho(V)$ are neglected, while those in $\mathbf{j}(V)$ are purely transverse and therefore do not contribute to the \overline{L}_1 RME. Note that the RMEs are purely real and in $\text{fm}^{3/2}$ units.

	$\overline{C}_1(q; V)$	$\overline{L}_1(q; V)$	$\overline{E}_1(q; V)$	$\overline{M}_1(q; A)$
one-body	-0.222×10^{-1}	-0.162×10^{-1}	-0.231×10^{-1}	-0.100×10^{-2}
mesonic	-0.222×10^{-1}	-0.209×10^{-1}	-0.298×10^{-1}	-0.779×10^{-3}
Δ			-0.298×10^{-1}	-0.809×10^{-3}

TABLE XIV. Cumulative contributions to the reduced matrix elements (RMEs) $\overline{C}_1(q; V)$, $\overline{L}_1(q; V)$, $\overline{E}_1(q; V)$ and $\overline{M}_1(q; A)$ in the 3P_1 capture at zero p ${}^3\text{He}$ c.m. energy. The momentum transfer q is 19.2 MeV/c, and the results correspond to the AV18/UIX Hamiltonian model. Notation as in Table XIII. Note that the RMEs are purely real and in $\text{fm}^{3/2}$ units.

	$\overline{C}_1(q; V)$	$\overline{L}_1(q; V)$	$\overline{E}_1(q; V)$	$\overline{M}_1(q; A)$
one-body	0.953×10^{-3}	0.118×10^{-2}	0.521×10^{-3}	0.304×10^{-1}
mesonic	0.217×10^{-2}	0.174×10^{-2}	0.128×10^{-2}	0.304×10^{-1}
Δ			0.127×10^{-2}	0.303×10^{-1}

TABLE XV. Cumulative contributions to the reduced matrix elements (RMEs) $\overline{C}_2(q; A)$, $\overline{L}_2(q; A)$, $\overline{E}_2(q; A)$ and $\overline{M}_2(q; V)$ in the 3P_2 capture at zero p ${}^3\text{He}$ c.m. energy. The momentum transfer q is 19.2 MeV/c, and the results correspond to the AV18/UIX Hamiltonian model. Notation as in Table IX. Note that the RMEs are purely imaginary and in $\text{fm}^{3/2}$ units.

	$\overline{C}_2(q; A)$	$\overline{L}_2(q; A)$	$\overline{E}_2(q; A)$	$\overline{M}_2(q; V)$
one-body	-0.146×10^{-3}	0.236×10^{-1}	0.292×10^{-1}	-0.110×10^{-2}
mesonic	-0.114×10^{-3}	0.236×10^{-1}	0.293×10^{-1}	-0.116×10^{-2}
Δ	-0.988×10^{-4}	0.238×10^{-1}	0.295×10^{-1}	-0.118×10^{-2}

TABLE XVI. Contributions of the S- and P-wave capture channels to the *hep* S -factor at zero p ${}^3\text{He}$ c.m. energy in 10^{-20} keV b. The results correspond to the AV18/UIX, AV18 and AV14/UVIII Hamiltonian models.

	AV18/UIX	AV18	AV14/UVIII
1S_0	0.02	0.01	0.01
3S_1	6.38	7.69	6.60
3P_0	0.82	0.89	0.79
1P_1	1.00	1.14	1.05
3P_1	0.30	0.52	0.38
3P_2	0.97	1.78	1.24
TOTAL	9.64	12.1	10.1

FIGURES

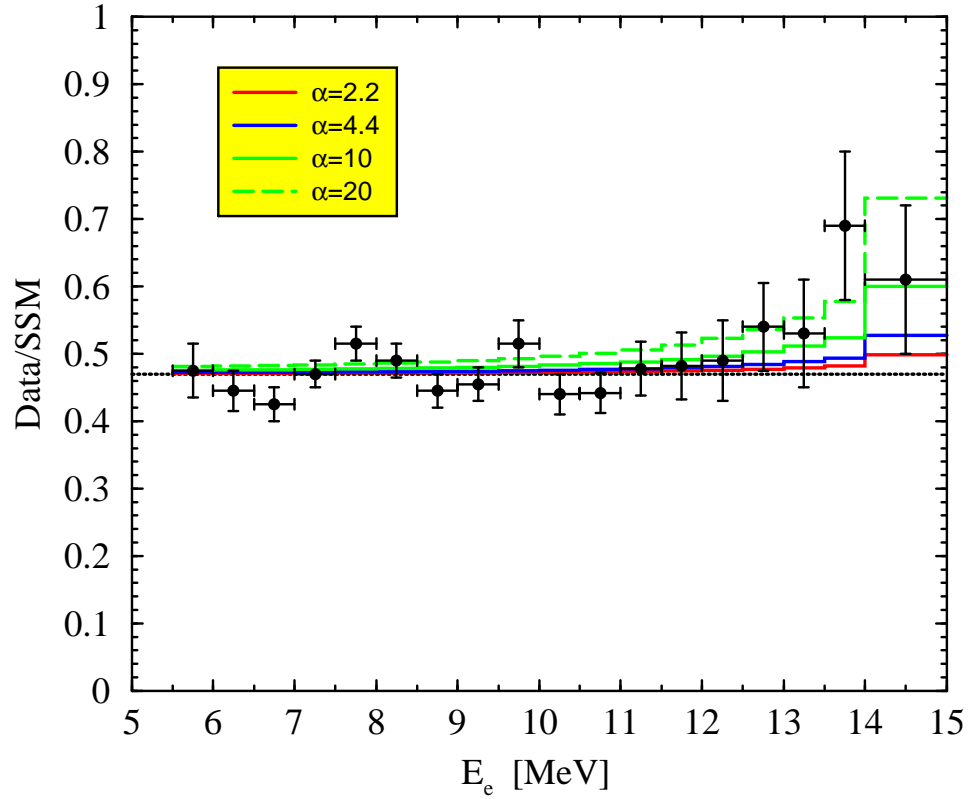


FIG. 1. Electron energy spectrum for the ratio between the Super-Kamiokande 825-days data and the expectation based on unoscillated ^8B neutrinos [10]. The data were extracted graphically from Fig. 8 of Ref. [9]. The 5 curves correspond respectively to no *hep* contribution (dotted line), and an enhancement α of 2.2 (solid red line), 4.4 (solid blue line), 10 (solid green line) and 20 (long-dashed green line).

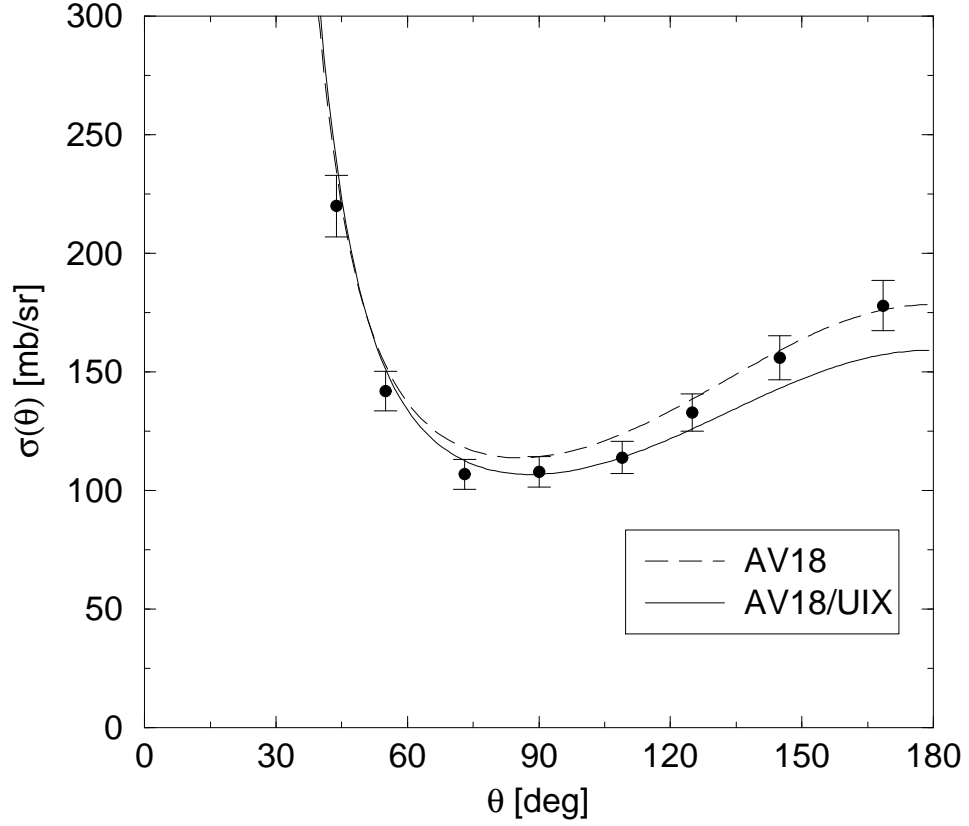


FIG. 2. Differential cross section $\sigma(\theta)$ as function of the c.m. scattering angle θ at c.m. energy of 1.2 MeV. The experimental data are taken from Ref. [62]. The long-dashed and solid lines correspond, respectively, to the CHH calculations with the AV18 and AV18/UIX Hamiltonian models.

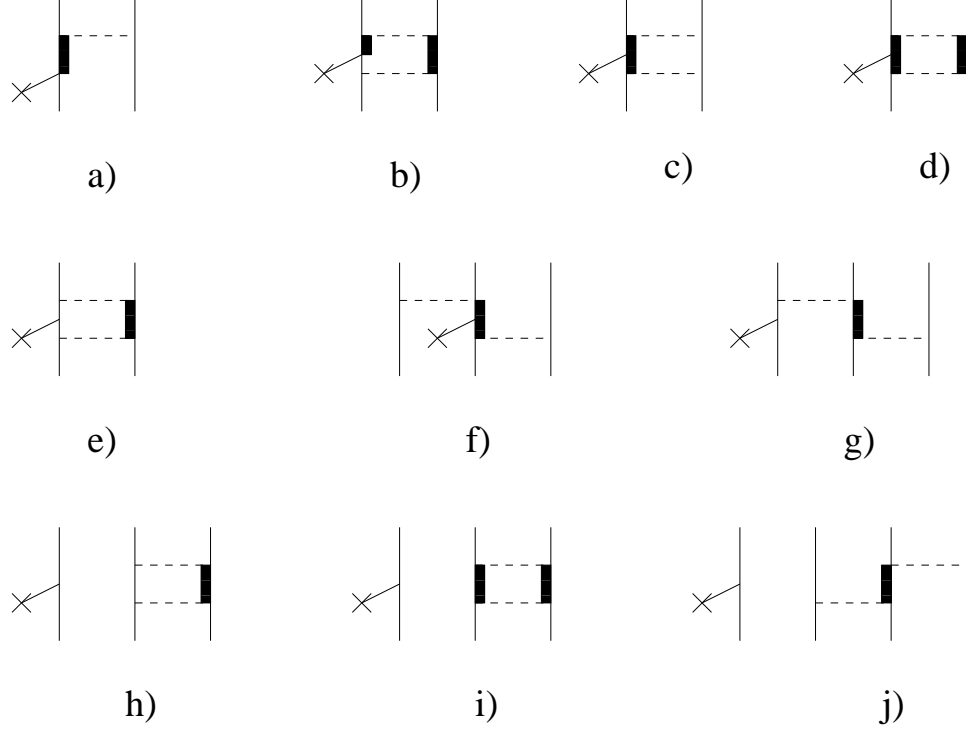


FIG. 3. Diagrammatic representation of the operators included in $O(\Delta)$, due to the one-body current and charge operators $O^{(1)}(N \rightarrow \Delta)$, $O^{(1)}(\Delta \rightarrow N)$, and $O^{(1)}(\Delta \rightarrow \Delta)$, given in Eqs. (4.48)–(4.53), and to the transition correlations $U^{\Delta N}$, $U^{N\Delta}$, $U^{\Delta\Delta}$, and corresponding hermitian conjugates. Thin, thick, and dashed lines denote, respectively, nucleons, Δ isobars, and transition correlations $U^{BB'}$ or $U^{BB'\dagger}$, with $B, B' \equiv N, \Delta$.

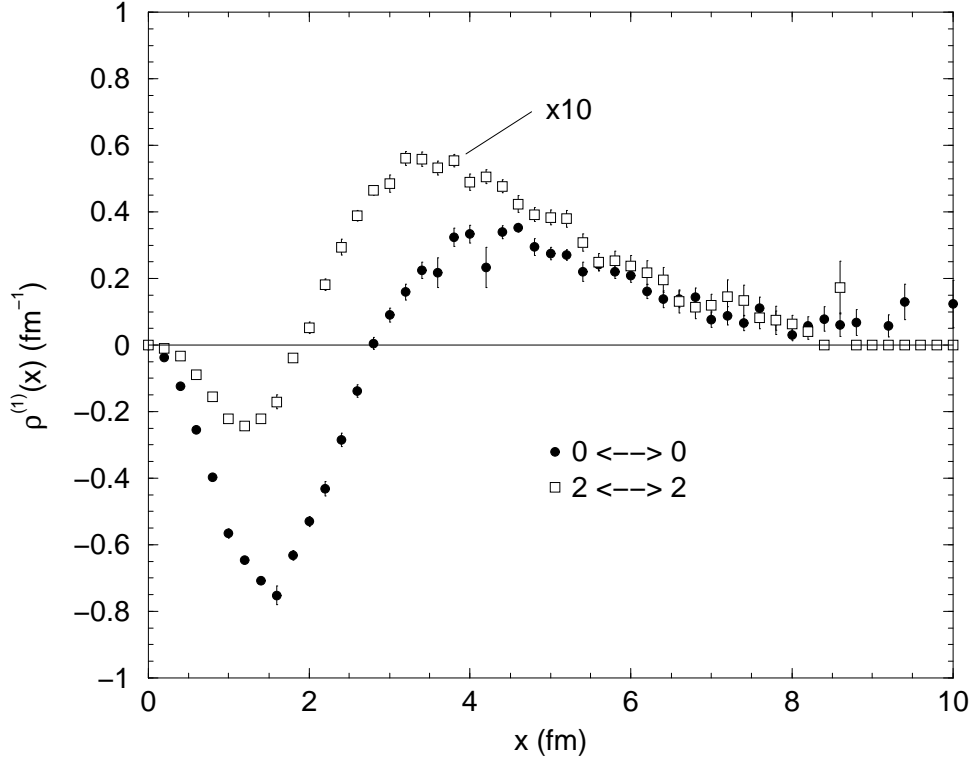


FIG. 4. Contributions to the density function $\rho^{(1)}(x)$, defined in Eq. (6.7), due to transitions involving the $L=0 \rightarrow L=0$ (filled circles) and $L=2 \rightarrow L=2$ (opaque squares) components in the ${}^3\text{He}$ and ${}^4\text{He}$ wave functions. Note that the $2 \rightarrow 2$ density function has been multiplied by a factor of 10, for ease of presentation.

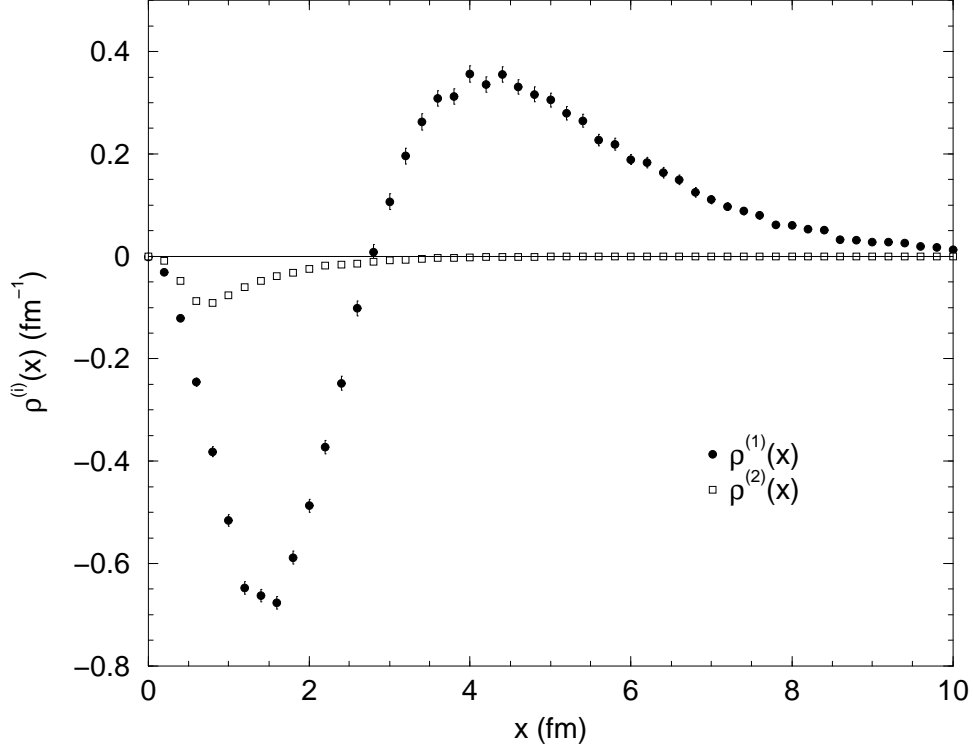


FIG. 5. Density functions $\rho^{(1)}(x)$ (filled circles) and $\rho^{(2)}(x)$ (opaque squares), defined in Eqs. (6.7)–(6.8).

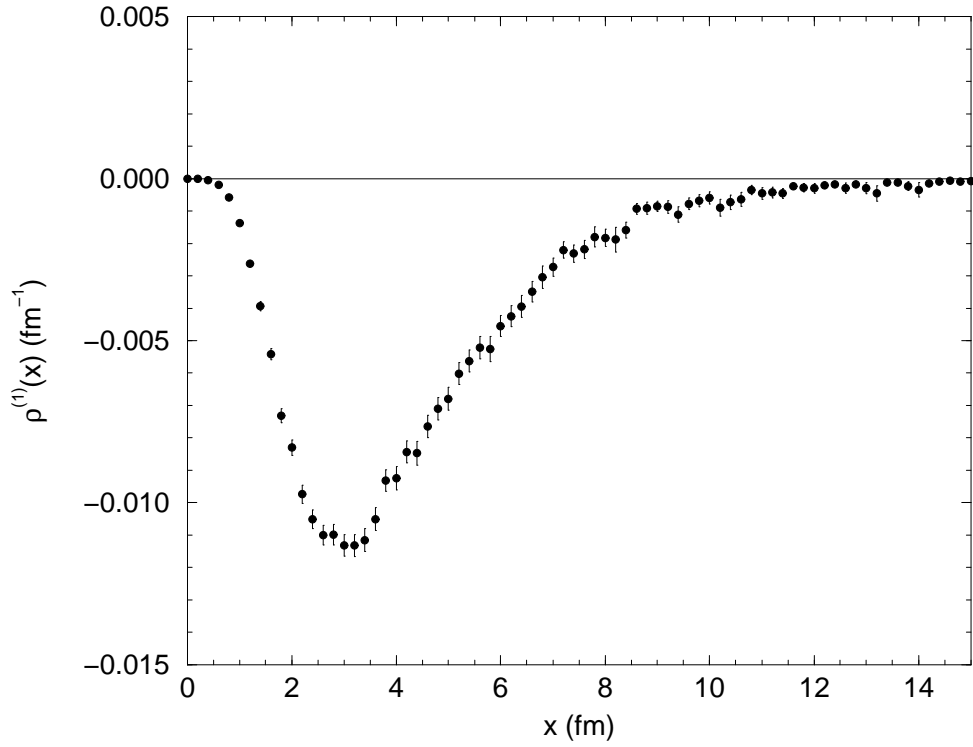


FIG. 6. Density function $\rho^{(1)}(x)$ defined in Eq. (6.7) in the 3P_2 capture channel.